Dynamic hidden-variable network models

Harrison Hartle, Fragkiskos Papadopoulos, and Dmitri Krioukov

Phys. Rev. E **103**, 052307 — Published 13 May 2021

DOI: 10.1103/PhysRevE.103.052307

Dynamic Hidden-Variable Network Models

Harrison Hartle,[1] Fragkiskos Papadopoulos,[2] and Dmitri Krioukov[1,3]

[1] *Network Science Institute, Northeastern University, Boston, MA, USA*
[2] *Department of Electrical Engineering, Computer Engineering and Informatics, Cyprus University of Technology, 3036 Limassol, Cyprus*
[3] *Northeastern University, Departments of Physics, Mathematics, and Electrical&Computer Engineering, Boston, MA, USA*

Models of complex networks often incorporate node-intrinsic properties abstracted as hidden variables. The probability of connections in the network is then a function of these variables. Real-world networks evolve over time, and many exhibit dynamics of node characteristics as well as of linking structure. Here we introduce and study natural temporal extensions of static hidden-variable network models with stochastic dynamics of hidden variables and links. The dynamics is controlled by two parameters: one that tunes the rate of change of hidden variables, and another that tunes the rate at which node-pairs re-evaluate their connections given the current values of hidden variables. Snapshots of networks in the dynamic models are equivalent to networks generated by the static models only if the link re-evaluation rate is sufficiently larger than the rate of hidden-variable dynamics, or, if an additional mechanism is added whereby links actively respond to changes in hidden variables. Otherwise, links are out of equilibrium with respect to hidden-variables and network snapshots exhibit structural deviations from the static models. We examine the level of structural persistence in the considered models and quantify deviations from static-like behavior. We explore temporal versions of popular static models with community structure, latent geometry, and degree heterogeneity. While we do not attempt to directly model real networks, we comment on interesting qualitative resemblances to real systems. In particular, we speculate that links in some real networks are out-of-equilibrium with respect to hidden variables, partially explaining the presence of long-ranged links in geometrically-embedded systems and inter-group connectivity in modular systems. We also discuss possible extensions, generalizations, and applications of the introduced class of dynamic network models.

I. INTRODUCTION

Networks are ubiquitous in nature [1–9], and their study relies heavily on the mathematical and computational analysis of simple models [10, 11], typically in the form of random networks built according to some stochastic rules. In many models, nodes are assigned characteristics (such as fitnesses [12, 13] or spatial coordinates in a physical [14] or latent space [15–17]), which in turn affect the network's structural formation. Such models fall under the umbrella of *hidden-variables* models [18], because they depend on internal node-characteristics that are only implicitly expressed by the network structure, through effects on link-formation. Usually, hidden variables (HVs) are not externally specified as parameters – rather, their probability distribution is specified [12, 19], and they are sampled during the network's formation. Two sources of randomness underly such networks: the random HVs of nodes, and the random formation of edges given those HVs. In general, hidden-variables models are defined by the following procedure:

1. A random hidden-variable configuration H is drawn with probability density $\rho(H)$ from a set of possible hidden-variable configurations $\mathcal{H}$.

2. Graph G is then drawn with conditional probability $\mathbb{P}(G|H)$ from a set of possible graphs $\mathcal{G}$.

As a result, the overall probability of sampling any particular graph $G \in \mathcal{G}$ is equal to

$$\mathbb{P}(G) = \int_{\mathcal{H}} \mathbb{P}(G|H)\rho(H)dH. \tag{1}$$

Hidden-variables models, due to their capacity to encode nodewise heterogeneity, are in many cases capable of exhibiting more structural realism than models without hidden variables. For example, hidden variables underly network models incorporating realistic features such as community structure (stochastic block models [20]), latent geometry (random geometric graphs [21]), and degree-heterogeneity (soft configuration models [22]).

However, such models do not capture the *dynamics* of node-characteristics, nor the impact thereof on network structure. The influence of dynamic node-states on evolving link-structure has been investigated in the context of *adaptive networks* [23–28], but in that case node-states arise due to a highly complex feedback, interacting with one another through co-evolving links. Such models are more realistic and have interesting features, but they do not directly explore the impact of dynamic node-properties on dynamic network structure.

There is a wide abundance of real-world examples of dynamic node-properties influencing dynamics of network structure, such as:

a) changing habits, interests, jobs, and other attributes of people in social networks [29],

b) changing geospatial coordinates of organisms during formation of social ties, group-memberships, and pathogenic contact networks [30–34],

c) changing phenotypic traits of species as they biologically evolve in ecological networks [35, 36],

d) changing marketing and administrative strategies of entities in economic networks [37, 38],

e) changing demographic and infrastructural characteristics of cities in evolving highway and airport networks [39–41],

f) changing gene-expression levels of neurons in developing connectomes [42, 43],

g) changing consumption-levels of residential nodes in evolving power grids [44, 45],

h) changing displayed content of websites on the evolving world-wide web [46, 47].

These examples motivate the development of a simple modeling framework describing the impact of dynamic node-characteristics on dynamic link-structure. Such a framework would provide a temporal analogue of how node-properties influence network structure in hidden-variables models. In fact, it is standard practice to derive temporal versions of static-network concepts [48–66], as has been done for several models of static networks with hidden variables such as stochastic block models [67–73].

Motivated by these considerations, here we study temporal extensions of general static hidden-variables models, obtained by introducing dynamics of hidden variables and of links. In these models each node has an evolving hidden variable, and each node-pair has a pairwise *affinity* (equal to the connection probability in the static hidden-variables model), which is a function of the hidden variables of both nodes. Pairwise affinities evolve over time due to their dependence on a pair of evolving hidden variables. The network itself evolves via node-pairs being selected to re-evaluate their connections, resampling them with connection probability equal to the pair's affinity at the moment of re-evaluation. These systems are governed by just two parameters beyond those of any static model: a rate of hidden-variable dynamics σ, and a rate of link-resampling ω.

We find that these models have snapshots that are statistically equivalent to networks generated from the static model if:

a) the link-resampling rate is sufficiently larger than the rate of hidden-variable dynamics, or

b) if we add an additional dynamic mechanism whereby links actively respond to changes in hidden variables.

We also identify the conditions under which model networks evolve *gradually*, *i.e.*, exhibit link-persistence, and evaluate qualitative resemblances of snapshots to some real networks which arise as *deviations* from static-model behavior. We obtain analytical and numerical results for effective connection probabilities (the probability of a node-pair being connected given their *current* hidden-variable values), directly quantifying deviations from static-model behavior in each case.

The family of models we introduce is demonstrated to have wide generality, as exemplified by temporal extensions of four different static models with hidden variables: stochastic block models [20], random geometric graphs [21], soft configuration models [22], and hyperbolic graphs [15]. These examples relate to, and partially encompass, several models of networks with dynamic node-properties that have been previously studied – for instance dynamic latent space models [74–77], dynamic random geometric graphs [78, 79], and dynamic stochastic block models [72, 73]. The framework we study is also widely generalizable to other contexts.

Our study takes a step towards realistic modeling of dynamic networks with dynamic node properties. It introduces a family of temporal network models that extends static hidden-variables models to the temporal setting, providing theoretical insight into the kinds of structure that can emerge as a consequence of the influence of hidden-variable dynamics on network-structure dynamics. The framework can be used for studying real-world temporal networks under the null hypothesis that physical or latent *dynamic* hidden variables drive the dynamics of network structure. Additionally, motivated by the phenomenology emerging in these models, we speculate that links in some real systems are *out of equilibrium* with respect to hidden-variables, partially explaining the presence of long-ranged links in geometrically-embedded systems and inter-group connectivity in modular systems.

In Section II, we describe the properties that we use to characterize the models we introduce. We then introduce the static and temporal hidden-variables model families in Section III, followed by various limiting regimes in Section IV. Section V provides several examples illustrating temporal hidden-variables models. We then consider a variant of the family of models in Section VI, incorporating an additional dynamic mechanism that enforces static-model connection probabilities. The final sections are dedicated to descriptions of related work (Section VII) and a discussion of our results and the implications thereof (Section VIII). Appendices provide the details of several calculations and procedures left out of the main text.

II. DESIRED PROPERTIES OF DYNAMIC HIDDEN-VARIABLES MODELS

This section outlines the properties that we use to characterize the family of dynamic hidden-variables models that we introduce. Our goal is to construct natural temporal versions of static networks with hidden variables, and to understand the consequences of having introduced

such dynamics. Our approach is via a Markov chain on graphs and hidden-variable configurations, with sources of randomness in the original static model being replaced by random *processes* in the temporal model.

Specifically, given a static hidden-variables model, *i.e.*, a probability density on hidden-variable configurations $H \in \mathcal{H}$ and a conditional probability distribution on graphs $G \in \mathcal{G}$ given H, the temporal extension yields a probability distribution/density on *temporal sequences* of graphs and hidden-variable configurations, denoted $\mathbf{G} = \left\{G^{(t)}\right\}_{t=1}^{T} \in \mathcal{G}^T$ and $\mathbf{H} = \left\{H^{(t)}\right\}_{t=1}^{T} \in \mathcal{H}^T$, respectively. We will evaluate the conditions under which models within our framework satisfy the following properties:

a) *Equilibrium Property:* The marginal probability of a graph at any timestep is identical to its probability in the static model; likewise for hidden variables.

b) *Persistence Property*: The level of structural persistence over time – quantified by, e.g., any graph similarity measure between graphs at adjacent timesteps – is high relative to the null expectation (of two i.i.d. static-model samples).

c) *Qualitative Realism*: The graph-structure, HV-geometry (e.g., link-lengths), and/or dynamic behaviors resemble observed characteristics of some real-world systems at a qualitative level.

If the Equilibrium Property is satisfied, the temporal network in question is a strict extension of the static model – individual snapshots are then indistinguishable from static-model realizations. If the Equilibrium Property is *not* satisfied, snapshots *deviate* from the static model, the resulting phenomenology of which we seek to understand. The Persistence Property holding implies a *gradually* evolving network, without sudden structural transitions between networks at adjacent timesteps. The Persistence Property can be quantified by application of graph similarity measures [80] to graphs at neighboring timesteps. In most cases the level of structural persistence is tunable, making the level of satisfaction of the Persistence Property fall along a continuum. The highest accessible persistence-values arise when the graph is completely unchanging over time, whereas the lowest accessible persistence-values correspond to graphs that are completely resampled each timestep. To have Qualitative Realism simply means that the system exhibits some characteristics and behaviors that are analogous to real-world systems – regardless of whether the detailed mechanisms are realistic or quantitatively accurate. In particular, we are interested in qualitative features relating to the dynamics of node-characteristics, and the effects of such dynamics on a network's structural evolution.

III. MODELING FRAMEWORK

This section provides an overview of our modeling approach, and then defines static and temporal hidden-variables models. We first describe our approach to constructing temporal extensions of static models, which produce length-T sequences of graphs $\mathbf{G}$ with a probability conditioned on a length-T sequence of hidden-variable configurations $\mathbf{H}$. The latter arises from Markovian dynamics [81, 82] governed by conditional probability density $\mathcal{P}_H\left(H^{(t+1)}\middle|H^{(t)}\right)$. The initial configuration $H^{(1)}$ is sampled from the static-model hidden-variable density $\rho\left(H^{(1)}\right)$. Markovian dynamics yields a temporally-joint probability density $p(\mathbf{H})$ as a product:

$$p(\mathbf{H}) = \rho\left(H^{(1)}\right)\prod_{t=1}^{T-1}\mathcal{P}_H\left(H^{(t+1)}\middle|H^{(t)}\right). \tag{2}$$

Given $\mathbf{H}$, the graph sequence $\mathbf{G}$ is produced via a Markov chain with transition probability having auxiliary $\mathbf{H}$-dependence, $\mathcal{P}_G\left(G^{(t+1)}\middle|G^{(t)},\mathbf{H}\right)$. Herein, we primarily consider graph dynamics with $\mathbf{H}$-dependence of the form $\mathcal{P}_G\left(G^{(t+1)}\middle|G^{(t)},H^{(t+1)}\right)$, but also consider dynamics of the form $\mathcal{P}_G\left(G^{(t+1)}\middle|G^{(t)},H^{(t+1)},H^{(t)}\right)$ in Section VI. In general, we could consider any choice of $\mathbf{H}$-dependence – as long as $G^{(t)}$ is not influenced by $H^{(t')}$ for any $t' > t$, since that would entail graph-structure at time t being dependent on HVs at future-times $t' > t$. The initial graph $G^{(1)}$ is sampled from the static-model conditional probability $\mathbb{P}\left(G^{(1)}\middle|H^{(1)}\right)$. The $\mathbf{H}$-conditioned temporally-joint graph probability distribution $P(\mathbf{G}|\mathbf{H})$ is then given by:

$$P(\mathbf{G}|\mathbf{H}) = \mathbb{P}\left(G^{(1)}\middle|H^{(1)}\right)\prod_{t=1}^{T-1}\mathcal{P}_G\left(G^{(t+1)}\middle|G^{(t)},\mathbf{H}\right). \tag{3}$$

Altogether, the temporally-joint graph probability distribution is given by

$$P(\mathbf{G}) = \int_{\mathcal{H}^T} P(\mathbf{G}|\mathbf{H})p(\mathbf{H})d\mathbf{H}, \tag{4}$$

which is the temporal extension of Equation (1).

It is this strategy that underlies all temporal extensions of static models that we consider. Static graphs without hyperparameters may also be included by disregarding $\mathbf{H}$ above, leaving only Equation (3), which becomes a general Markov chain on graphs governed by $\mathcal{P}_G\left(G^{(t+1)}\middle|G^{(t)}\right)$. Note that $\mathbf{G}$ can be seen as a multiplex network [83, 84] with layers representing timesteps.

A. Static Hidden-Variables Model

Here we describe the static hidden-variables model [18] (SHVM), which generates graphs by a two-step procedure. First, each node j (out of n total, labeled as

$\{1, ..., n\} = [n]$) is assigned a *hidden variable* $h_j \in \mathcal{X}$, drawn independently with probability density $\nu(h_j)$ from set $\mathcal{X}$. Thus the hidden-variable configuration is $H = \{h_j\}_{j=1}^n \in \mathcal{H} = \mathcal{X}^n$ and the joint hidden-variable density is $\rho(H) = \prod_{j=1}^n \nu(h_j)$. Second, node-pairs ij $(1 \leq i < j \leq n)$ connect with pairwise probability $f(h_i, h_j)$, independently from one another. The conditional probability $\mathbb{P}(G|H)$ of a graph G is thus given by

$$\mathbb{P}(G|H) = \prod_{1 \leq i < j \leq n} \left(f(h_i, h_j)\right)^{A_{ij}} \left(1 - f(h_i, h_j)\right)^{1 - A_{ij}}, \tag{5}$$

where $\{A_{ij}\}_{1 \leq i < j \leq n}$ are elements of the adjacency matrix of graph G. For a fixed H, this is an edge-independent random graph. But since H is random, $\mathbb{P}(G)$ is a probabilistic mixture of Equation 5 over possible hidden-variable configurations $H \in \mathcal{X}^n$ via Equation 1.

B. Temporal Hidden-Variables Model

We now describe a temporal version of the SHVM (Section III A), namely the *temporal hidden-variables model* (THVM). We denote by $A_{ij}^{(t)}$ the ij-th element of $G^{(t)}$'s adjacency matrix. The initial conditions $(G^{(1)}, \{h_j^{(1)}\}_{j=1}^n)$ are sampled from the SHVM. For $t \in \{1, ..., T-1\}$, the system updates according to:

a) *Hidden-variable dynamics:* Each node j samples $h_j^{(t+1)}$ from a conditional density $\mathcal{P}_h(h_j^{(t+1)}|h_j^{(t)})$, discussed below.

b) *Link-resampling:* Each node-pair ij, with probability ω, resamples $A_{ij}^{(t+1)}$ with connection probability $f(h_i^{(t+1)}, h_j^{(t+1)})$. Otherwise, $A_{ij}^{(t+1)} = A_{ij}^{(t)}$.

Simply put, each node's hidden variable undergoes Markovian dynamics (governed by $\mathcal{P}_h$), and each node-pair ij is re-evaluated for linking (with probability ω each timestep) with connection probability equal to ij's current affinity-value $f(h_i^{(t+1)}, h_j^{(t+1)})$. We separately consider two types of hidden-variable dynamics $\mathcal{P}_h$:

a) *Jump-dynamics:* Each node j, with probability $\sigma \in [0, 1]$, resamples its hidden-variable to obtain $h_j^{(t+1)}$. The conditional density for jump-dynamics is thus

$$\mathcal{P}_h(h'|h) = \sigma\nu(h') + (1 - \sigma)\mathbf{1}_h(h'), \tag{6}$$

with $\mathbf{1}_h(h')$ being the Dirac measure.

b) *Walk-dynamics:* The hidden variable of every node moves to a nearby point in $\mathcal{X}$ using Brownian-like motion with the average step-length proportional to parameter $\sigma \in [0, 1]$.

We implement the latter option by transforming the density $\nu(h)$ on $\mathcal{X}$ to the uniform density on $[0, 1]^D$, where D is the dimension of $\mathcal{X}$, using the inverse CDF transform. We then do a random walk in $[0, 1]^D$, with step-size proportional to σ, preserving the uniform distribution. Transformed back to $\mathcal{X}$, the random walk increments preserve the distribution $\nu(h)$. The details are in Appendix D.

In both walk-dynamics and jump-dynamics, parameter σ encodes the rate of change of hidden variables. Also in both cases, the transition probability density $\mathcal{P}_H$ is separable due to independence of $\{h_j^{(t)}\}_{j=1}^n$:

$$\mathcal{P}_H\left(H^{(t+1)}\middle|H^{(t)}\right) = \prod_{j=1}^n \mathcal{P}_h\left(h_j^{(t+1)}\middle|h_j^{(t)}\right). \tag{7}$$

The stationary density of the above dynamics is equal to the static-model hidden-variable density ρ. The density of $\mathbf{H} = \{\{h_j^{(t)}\}_{j=1}^n\}_{t=1}^T$ is also separable,

$$p(\mathbf{H}) = \prod_{j=1}^n \left(\nu\left(h_j^{(1)}\right) \prod_{t=1}^{T-1} \mathcal{P}_h\left(h_j^{(t+1)}\middle|h_j^{(t)}\right)\right). \tag{8}$$

The probability of a graph-sequence $\mathbf{G}$ given $\mathbf{H}$ is the temporal product (3) of the following transition probabilities,

$$\mathcal{P}_G\left(G^{(t+1)}\middle|G^{(t)}, H^{(t+1)}\right) = \prod_{1 \leq i < j \leq n} Y_{ij}^{A_{ij}^{(t+1)}} (1 - Y_{ij})^{1 - A_{ij}^{(t+1)}}, \tag{9}$$

with Y_{ij} denoting the conditional linking probability,

$$Y_{ij} = \omega f\left(h_i^{(t+1)}, h_j^{(t+1)}\right) + (1 - \omega)A_{ij}^{(t)}, \tag{10}$$

encoding the fact that link-resampling happens with probability ω, and that otherwise the link (or non-link) remains the same.

We will primarily quantify the structure of THVM snapshots via the *effective connection probability*,

$$\bar{f}(h, h') = \lim_{t \to \infty} \mathbb{P}\left(A_{ij}^{(t)} = 1 \middle| h_i^{(t)} = h, h_j^{(t)} = h'\right), \tag{11}$$

which, if the Equilibrium Property is satisfied, is the same as the affinity-function $f(h, h')$. If the affinity is a function of a composite variable such as the distance between or the product of the pair of hidden variables, the effective connection probability is defined analogously but for those composite quantities. We note here that the average degree (number of link-ends per node) is independent of the values of σ and ω in THVM snapshots (see Appendix A).

IV. PARAMETER SPACE AND RESULTING DYNAMICS OF TEMPORAL HIDDEN VARIABLES MODELS

In this section we consider several limiting cases in the space of dynamics-parameters $(\sigma, \omega) \in [0, 1]^2$, and

Name	Parameter Regime	Equilibrium Property	Tunable Persistence
Single Static Graph	$\omega = \sigma = 0$	Yes	No
i.i.d. Graph Sequence	$\omega = \sigma = 1$	Yes	No
Quasi-Static	$\alpha_2(\sigma, \omega) \approx 1$ (Equation 12)	Yes*	Yes
Complete link-resampling	$\omega = 1, \sigma \in (0, 1)$	Yes	Depends on f**
Deterministic HV-to-graph	$\omega = 1, f : \mathcal{X}^2 \to \{0, 1\}$	Yes	Depends on f**
Complete HV-resampling	$\sigma = 1, \omega \in (0, 1)$	No	Yes ***
Fixed Hidden Variables	$\sigma = 0$	Yes	Yes
Erdős-Rényi-like	$\sigma/\omega \gg 1$	No	No
Fixed graph structure	$\omega = 0$	Yes****	No****

TABLE I. **Table of limiting cases of dynamics-parameters (σ, ω) for THVMs.** The first and second columns provide a short-hand name and the associated parameter regime. The third column states whether the Equilibrium Property is satisfied, whereas the fourth column states whether the Persistence Property is satisfied (in a way that is tunable at any desired level, which for instance leaves out the case $\sigma = \omega = 0$).

*In the quasi-static regime, $G^{(t)}$ will have arisen from an HV-configuration closely resembling $H^{(t)}$, due to a timescale-separation. This implies *approximate*, rather than exact, satisfaction of the Equilibrium Property.

** When $\omega = 1$ although the persistence property is in general lost due to each possible edge being resampled at every timestep, there is still *some* persistence present, tuned by σ and dependent upon the affinity function f.

*** When $\sigma = 1$ the persistence property is tunably satisfied at the level of graph-structure, but not at all at the level of hidden variables, which are completely resampled every timestep.

**** In the case of $\omega = 0$, the initial graph remains fixed for all time, while HVs change. Since the initial condition is sampled from the static model, this regime technically satisfies the Equilibrium Property. It does so both at the level of graphs and at the level of hidden variables, but not at all at the *joint* level. Persistence is not tunable at the level of graphs, but is at the level of hidden variables.

some special-case categories of affinity function f. The resulting regimes exhibit a variety of qualitatively distinct behaviors. If $\sigma = \omega = 0$, a single graph is sampled from the static model, and all of its hidden variables and links are held fixed for all t. To the opposite extreme, if $\sigma = \omega = 1$, at each timestep, every node's hidden variable is fully randomized, and then all possible links are re-evaluated, resulting in a sequence of independent and identically distributed (i.i.d.) instances of the static model. In either case, the Equilibrium Property is satisfied – but the Persistence Property is not for $\sigma = \omega = 1$ (there is no persistence), whereas for $\sigma = \omega = 0$ there is complete persistence.

In Sections IV A, IV B, IV D, and IV C, several other parameter regimes are analyzed. We discuss the behavior of temporal networks in each case, how well they qualify in terms of the Equilibrium and Persistence Properties, and their relations to preexisting commonly studied static network ensembles. Table I shows the different special cases, while a schematic picture of the space of dynamics-parameters is shown in Figure 1.

A. Quasi-Static Regime ($\alpha_2(\sigma, \omega) \approx 1$)

Here we consider the parameter regime quantified by the condition $\alpha_2(\sigma, \omega) \approx 1$ (upper-left region of Figure 1), where

$$\alpha_2(\sigma, \omega) = \frac{\omega}{1 - (1 - \omega)(1 - \sigma)^2} \in [0, 1], \qquad (12)$$

in which networks have both random link-structure and random hidden variables, and exhibit both the Persistence Property and the Equilibrium Property. The quantity $\alpha_2(\sigma, \omega)$ is a naturally-arising function characterizing how effective connection probabilities differ from their static-model counterparts (see Appendix A). The Equilibrium Property is satisfied due to sufficient timescale separation: link-resampling happens quickly enough relative to hidden-variable motion for $G^{(t)}$ to remain caught up with $H^{(t)}$. The dynamics can thus be considered quasi-static, in the sense of quasi-static transformations in classical equilibrium thermodynamics [85]. Over time, the HV-configuration and link-structure both fully explore their respective spaces, functioning as a temporal network whose stationary distribution is the static hidden-variables model defined in Section III A. Note that the Equilibrium Property is only *approximately* satisfied if $\alpha_2(\sigma, \omega) < 1$, that approximation becoming exact only in limit of extreme timescale-separation or $\alpha_2(\sigma, \omega) = 1$. Two regimes at the boundary of the quasi-static regime have exact satisfaction of the Equilibrium Property: $\omega = 1$ (Section IV B) and $\sigma = 0$ (Section IV C). Adding a third mechanism of dynamics allows for exact satisfaction of the Equilibrium Property at all $(\sigma, \omega) \in [0, 1]^2$ (see Section VI).

B. Complete link-resampling ($\omega = 1$)

Here we consider the case $\omega = 1$ (top region of Figure 1). This case resembles that of the quasi-static regime, but all links form based on *current* hidden-variable configurations, so there is no graph-encoded memory: $\mathcal{P}_G\left(G^{(t+1)} \middle| G^{(t)}, \mathbf{H}\right) = \mathbb{P}\left(G^{(t+1)} \middle| H^{(t+1)}\right)$. The resulting Markov chain on $\mathcal{H} \times \mathcal{G}$ thus satisfies the Equilibrium Property *exactly*, as opposed to approximately in the quasi-static regime (Subsection IV A). Link-structure

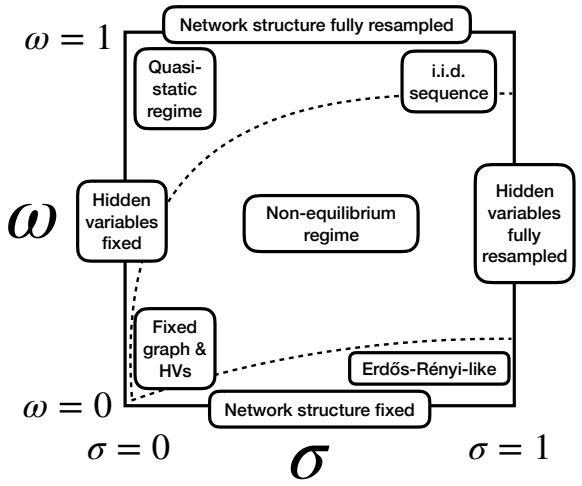

FIG. 1. **Two-parameter space of possible dynamics.** The two parameters $(\sigma, \omega) \in [0,1]^2$ tune the rate of change of hidden variables and rate of resampling of links, respectively. In general, with dynamic hidden variables, link-structure is out-of-equilibrium relative to the configuration of hidden variables at any particular timestep, violating the Equilibrium Property. In the quasi-static regime (upper left) and along the upper and leftward boundary regions ($\omega = 1$ and $\sigma = 0$, respectively) the Equilibrium Property is recovered. In the lower-right regime, HVs are so randomized that network snapshots resemble Erdős-Rényi graphs. At $\sigma = 1$ (right-hand boundary), all hidden variables are resampled at every timestep, but only a fraction ω of links resampled. If $\omega = 0$ (lower boundary), the network structure remains fixed for all time, regardless of the hidden-variable dynamics. The dashed curves distinguish, qualitatively, three regimes: the quasi-static regime lies above the upper dashed curve, the Erdős-Rényi-like regime lies below the lower dashed curve, and the general non-equilibrium regime lies in between. The shapes of the dashed curves come from contours of the function $\alpha_2(\sigma, \omega)$: the upper curve approximately designates $\alpha_2(\sigma, \omega) = 0.85$, whereas the lower curve approximately designates $\alpha_2(\sigma, \omega) = 0.15$ (see Section IV A and Figure 3). Both curves emanate from $(0, 0)$ and reach the $\sigma = 1$ boundary at the values of $\alpha_2(1, \omega) = \omega \approx 0.85$ (upper curve) and $\alpha_2(1, \omega) = \omega \approx 0.15$ (lower curve), see Equation 12.

when $\omega = 1$ is more correlated over time than two i.i.d. samples from the SHVM (due to persistence in HV-configurations), but the specific level of persistence depends on the form of the affinity function $f(h, h')$ and on σ. A variety of temporal network models have fully-resampled edges at each timestep [72, 86, 87].

As subset of the $\omega = 1$ regime, consider THVMs with binary affinity function $f : \mathcal{X}^2 \to \{0, 1\}$. In this case *all randomness comes from hidden variables*, because f deterministically maps HV-configurations to graphs. The static model's conditional probability distribution in such cases is given by a product of indicator functions:

$$\mathbb{P}(G|H) = \prod_{1 \le i < j \le n} \mathbf{1}\left\{A_{ij} = f\left(h_i, h_j\right)\right\}, \tag{13}$$

equal to 1 if and only if $f(h_i, h_j) = A_{ij}$ for all ij, and equal to zero otherwise. Since the HV-dynamics $\mathcal{P}_H$ conserves ρ, and since $\omega = 1$ ensures that all node-pairs have up-to-date links with respect to hidden variables, this model satisfies the Equilibrium Property *exactly*. The rate of HV-dynamics, and thus of link-dynamics, is controlled by σ (but also influenced by the form of f). This regime encompasses sharp random geometric graphs (RGGs) of any kind [21]; see Section V B for temporal RGGs with $\omega \in [0, 1]$.

C. Fixed Hidden Variables ($\sigma = 0$)

Here we consider $\sigma = 0$ (left region of Figure 1), in which case all HVs are frozen in place, ensuring satisfaction of the Equilibrium Property. The initial HV-configuration $H^{(1)}$ has the SHVM density ρ, but conditioning on some particular initial configuration $H^{(1)}$ yields fixed pairwise connection probabilities $p_{ij} = f\left(h_i, h_j\right)$, resulting in temporal versions of edge-independent static networks [88–90]. Analytical expressions for link-dynamics can be written straightforwardly in terms of the set of values $\{p_{ij}\}_{1 \le i < j \le n}$ and the parameter ω. The transition probability $\mathcal{P}_G\left(G^{(t+1)} \middle| G^{(t)}\right)$ is

$$\mathcal{P}_G(G^{(t+1)}|G^{(t)}) = \prod_{1 \le i < j \le n} p_{ij}^{A_{ij}^{(t)} \to A_{ij}^{(t+1)}}, \tag{14}$$

where $p_{ij}^{0\to0}$, $p_{ij}^{0\to1}$, $p_{ij}^{1\to0}$, and $p_{ij}^{1\to1}$ are respectively the non-link persistence, link-formation, link-removal, and link-persistence probabilities for node-pair ij. That is, $p_{ij}^{\alpha\to\beta} = \mathbb{P}(A_{ij}^{(t+1)} = \beta | A_{ij}^{(t)} = \alpha)$, given by:

$$\begin{aligned} p_{ij}^{\alpha\to\beta} =& (1 - \omega p_{ij})^{(1-\alpha)(1-\beta)} (\omega p_{ij})^{(1-\alpha)\beta} \\ & \times (\omega(1 - p_{ij}))^{\alpha(1-\beta)} (1 - \omega(1 - p_{ij}))^{\alpha\beta}. \end{aligned} \tag{15}$$

Many static network models have independent edges with pre-defined connection probabilities, and thus can be made temporal as THVMs with $\sigma = 0$. Examples include the Erdős-Rényi (ER) model [91] the (soft) stochastic block model (SBM) [92], and inhomogeneous random graphs [88] with fixed coordinates.

The Persistence Property can be quantified by any of the numerous measures of graph dissimilarity [80], by application to graph-pairs at neighboring timesteps. A simple example in the $\sigma = 0$ setting is the expected Ham-

ming dissimilarity [93],

$$\sum_{1\le i<j\le n} \mathbb{P}\left(A_{ij}^{(t)} \neq A_{ij}^{(t+1)}\right) = \sum_{1\le i<j\le n} \left(p_{ij}^{1\to 0} p_{ij} + p_{ij}^{0\to 1}(1-p_{ij})\right) = 2\omega \sum_{1\le i<j\le n} p_{ij}(1-p_{ij}), \tag{16}$$

which simplifies substantially in some cases, for instance the ER model ($p_{ij} = p$ for all ij), leaving $2\omega p(1-p)\binom{n}{2}$. The parameter ω directly tunes the level of persistence, with $\omega = 0$ yielding the highest persistence (an unchanging graph) and $\omega = 1$ yielding the lowest persistence (a fully resampled graph).

Edge-resampling dynamics with fixed p_{ij}-values closely resembles *dynamic percolation* [94], which has been investigated in lattices [95], trees [96] and ER graphs [97, 98], and also relates to *edge-Markovian networks* [99–101].

D. Complete resampling of hidden variables ($\sigma = 1$)

Here we consider the case for which all hidden variables are resampled at every timestep ($\sigma = 1$), so that no HV-driven structural persistence exists (right region of Figure 1). Note that walk-dynamics is parameterized by σ so that $\sigma = 1$ implies complete HV-randomization. If $\sigma = 1$, correlations among links (and non-links) do still exist due to simultaneous resampling; the set of node-pairs selected for link-resampling at timestep t form links based upon the *same* underlying hidden-variable configuration $H^{(t)}$. In this setting, ω quantifies the level of agreement among node-pairs as to what the HV-configuration is. For instance in spatial network models, if $\sigma = 1$, then ω directly controls the level of geometry-induced correlations.

Given the HV-configuration at time t and averaging over all past timesteps, node-pair ij is connected with probability

$$\mathbb{P}\left(A_{ij}^{(t)} = 1 \,\middle|\, h_i^{(t)}, h_j^{(t)}\right) = \omega f\left(h_i^{(t)}, h_j^{(t)}\right) + (1-\omega)\langle f\rangle, \tag{17}$$

where $\langle f\rangle = \int_{\mathcal{X}^2} \nu(h)\nu(h') f(h,h') dh dh'$ is the expected affinity of a pair of nodes with randomized HVs. The expression 17 is an example of an effective connection probability which deviates from the static-model affinity function. A more general formula for the effective connection probability in the case of jump-dynamics and arbitrary $f(h,h')$, σ, and ω is derived in Appendix A, and some special cases are described in the examples in Sections V A,V B,V C,V D. As $\omega \to 0$ with $\sigma = 1$ (and in general for $\sigma/\omega \gg 1$), the model approaches a temporal version of the ER model, since each node-pair at the time of link-resampling will have completely randomized hidden variables; each edge will then independently exist with probability $\langle f\rangle$ if $0 < \omega \ll 1$. If $\omega = 0$ we have fixed graph structure, *i.e.* a network that simply remains as whatever the initially sampled graph was, but with dynamic hidden variables (for any $\sigma > 0$).

V. TEMPORAL EXTENSIONS OF POPULAR STATIC NETWORK MODELS

This section contains several examples of THVMs. In each subsection, we describe a static hidden-variables model, its temporal extension according to the modeling framework of Section III B, the effective connection probability that arises due to the dynamics, and offer some additional discussion. We specifically consider temporal extensions of the following static network models: stochastic block models [20], random geometric graphs [21], hypersoft configuration models [22], and hyperbolic graphs [15].

A. Temporal Stochastic Block Models

This subsection considers temporal extensions of stochastic block models (SBMs), which are used to model community structure in networks [20, 92, 102, 103].

1. *Static Hyperparametric SBMs*

We consider a static network with conditionally Bernoulli-distributed edges amongst n nodes $j \in [n]$, each node having been randomly assigned to one of m groups (a.k.a. communities, blocks, colors). Each node j independently draws a group-index $q_j \in [m] = \{1, ..., m\}$ from probability distribution $\varrho = \{\varrho_q\}_{q\in[m]}$. Each node-pair then connects with probability f_{q_i,q_j}. In this definition, the group-memberships $\{q_j\}_{j\in[n]}$ are not externally specified as model parameters – rather, their distribution ϱ is specified. Thus, the group-memberships are hyperparameters, and we refer to these static networks as hyperparameteric SBMs or hyper-SBMs (equivalent to inhomogeneous random graphs with hidden color [105, 106]). The expected number of nodes n_q in a given block q is $\langle n_q\rangle = n\varrho_q$, and the joint distribution of $\{n_q\}_{q\in[m]}$ is multinomial. Note that this model could be formulated with continuous HVs as per Section III A, but we instead use discrete HVs for simplicity (see Appendix H for the continuous-to-discrete mapping). As an illustrative example to be used throughout this section, we consider the case of $m = 2$ groups, with $\varrho_1 = 1 - \varrho_2 = u$. The within-group affinity is $p = f_{1,1} = f_{2,2}$, and the between-group affinity is zero ($f_{1,2} = 0$).

2. *Temporal hyper-SBMs*

To make the hyper-SBM dynamic, at each timestep $t \in \{2, ..., T\}$ each node i with probability σ resamples its

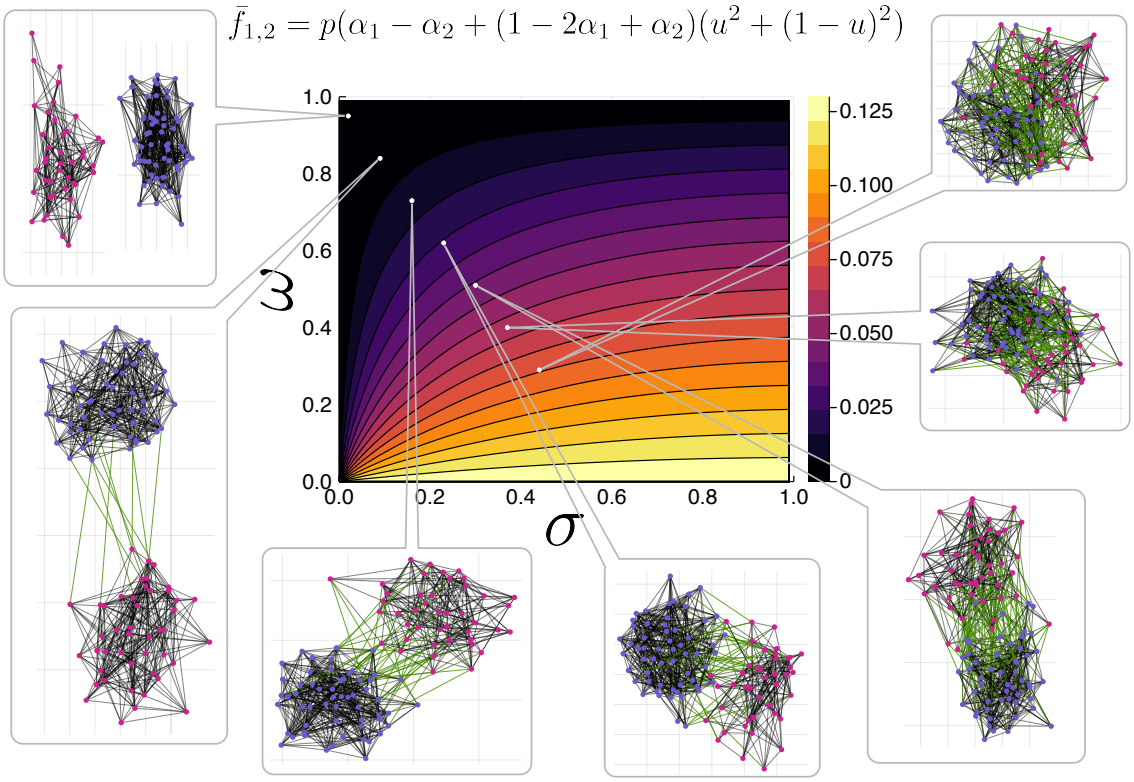

FIG. 2. **Snapshots of a temporal stochastic block model: a modular network with dynamic group-assignments and link-resampling.** The $n = 100$ nodes are partitioned into two groups with group-membership probabilities $\varrho_1 = 0.4 = 1-\varrho_2$, and group-memberships change in time by group-resampling with probability σ. The affinity function is $f_{q,q'} = p\mathbf{1}\{q = q'\}$ with $p = 0.25$, disallowing inter-group connections in the *static* model. Network snapshots are displayed via a spring-force layout algorithm [104], for various parameters (σ, ω) such that networks span a variety of structural outcomes. **Node-coloration** is by group-membership, and **link-coloration** is black for within-group links and green for between-group links. In the **central panel**, the effective connection probability $\bar{f}_{1,2}$ between communities is plotted. Outside of the quasi-static regime, group-membership dynamics is fast enough for a substantial number of inter-group links to exist ($\bar{f}_{1,2} > 0$), despite the inter-group connection *formation* probability being $f_{1,2} = 0$.

group-index $q_i^{(t)}$ from distribution ϱ, and then each node-pair ij with probability ω resamples $A_{ij}^{(t)}$ with connection probability $f_{q_i^{(t)},q_j^{(t)}}$. Thus,

$$\mathbb{P}\left(q_i^{(t)} = q' \,\middle|\, q_i^{(t-1)} = q\right) = (1-\sigma)\mathbf{1}\{q = q'\} + \sigma\varrho_{q'}, \quad (18)$$

and

$$\mathbb{P}\left(A_{ij}^{(t)} = 1 \,\middle|\, A_{ij}^{(t-1)}, q_i^{(t)}, q_j^{(t)}\right) = (1-\omega)A_{ij}^{(t-1)} + \omega f_{q_i^{(t)},q_j^{(t)}}. \quad (19)$$

See Figure 2 for visualized embeddings of network snapshots from the stationary distribution of the example $m = 2$, $\varrho_1 = u = 1 - \varrho_2$, $f_{q,q'} = p\mathbf{1}\{q = q'\}$.

3. *Effective connection probabilities in hyper-SBMs*

The block-dynamics of nodes in temporal hyper-SBMs introduces several novel features to the system. First, pairwise affinities change over time. Second, the set of all existing links at time t need not have arisen from the group-assignments of time t. Temporal snapshots in general thus deviate from the static model – the Equilibrium Property does not necessarily hold. However, even if snapshots do not resemble *the* static model, they do resemble *a* static model – an *effective* SBM. Consider two nodes, with current group-indices q, q'. Averaging over all past values of hidden variables, we obtain the effective connection probability $\bar{f}_{q,q'}$ for dynamic hyper-SBMs. Since the SBM case is directly obtainable from

discretization of the continuous model (see Appendix H) we can use a discrete version of the general formula derived in Appendix A, namely:

$$\begin{aligned}\bar{f}_{q,q'} &= \alpha_2 f_{q,q'} \\ &+ (\alpha_1 - \alpha_2)\left(\langle f_{q,\cdot}\rangle + \langle f_{q',\cdot}\rangle\right) \\ &+ (1 - 2\alpha_1 + \alpha_2)\langle f\rangle,\end{aligned} \tag{20}$$

where coefficients $\alpha_b(\sigma,\omega)$ for $b \in \{1,2\}$ are given by

$$\alpha_b = \frac{\omega}{1-(1-\omega)(1-\sigma)^b}, \tag{21}$$

and marginally-averaged affinities are

$$\begin{aligned}\langle f_{q,\cdot}\rangle &= \sum_{q'} \varrho_{q'} f_{q,q'}, \\ \langle f\rangle &= \sum_{q} \varrho_q \langle f_{q,\cdot}\rangle = \sum_{q,q'} \varrho_q \varrho_{q'} f_{q,q'}.\end{aligned} \tag{22}$$

Note that when $\sigma = 1$ we have $\alpha_1(1,\omega) = \alpha_2(1,\omega) = \omega$ and Equation 20 reduces to the form of Equation 17. In the simple example case ($m = 2, \varrho_1 = u, f_{q,q'} = p\mathbf{1}\{q = q'\}$), terms in $\bar{f}_{q,q'}$ are evaluated as:

$$\begin{aligned}\langle f_{1,\cdot}\rangle &= up, \\ \langle f_{2,\cdot}\rangle &= (1-u)p, \\ \langle f\rangle &= p(u^2 + (1-u)^2),\end{aligned} \tag{23}$$

from which the formula for $\bar{f}_{q,q'}$ becomes

$$\begin{aligned}\bar{f}_{q,q'} &= \alpha_2 p\mathbf{1}\{q = q'\} \\ &+ (\alpha_1 - \alpha_2)\begin{cases} 2up, & q = q' = 1 \\ 2(1-u)p, & q = q' = 2 \\ p & q \neq q' \end{cases} \\ &+ (1 - 2\alpha_1 + \alpha_2)p(u^2 + (1-u)^2).\end{aligned} \tag{24}$$

In particular, the between-group effective connection probability becomes

$$\bar{f}_{1,2} = p\left(\alpha_1 - \alpha_2 + (1 - 2\alpha_1 + \alpha_2)(u^2 + (1-u)^2)\right), \tag{25}$$

which is visualized in Figure 2. In the extreme case of $\sigma/\omega \gg 1$ all links form between nodes with effectively random group-assignments, making all pairs equally likely to connect, and reducing the system to a temporal Erdős-Rényi network of connection probability $p(u^2 + (1-u)^2)$.

4. *Temporal hyper-SBMs discussion*

Interesting examples of Qualitative Realism arise in temporal hyper-SBMs. For instance, group-dynamics of nodes yields inter-group connectivity, as is observed in real systems. If someone joins a different club, switches political party, or emigrates to a new country, they at first primarily carry ties to their original group – and thus upon changing group-membership, they suddenly have many inter-group links – *not* because of inter-group link-formation, but because of dynamic group-membership. Likewise, within-group connectivity can be *lower* than in the static model, as is the case in real systems due to nodes having recently arrived from another group, or from neighbor-nodes having recently departed. These effects arise *outside* the quasi-static regime, so we speculate that in some cases the *non-equilibrium* regime can better emulate real-world systems. We also note that we here considered group-resampling HV-dynamics (a discrete version of jump-dynamics), but we could also consider a general Markov chain on group-assignments with stationary distribution ϱ.

B. Temporal Random Geometric Graphs

In this section we describe THVMs arising from static random geometric graphs (RGGs), which model the influence of an underlying geometry on graph-structure [21].

1. *Static Random Geometric Graphs*

In random geometric graphs (RGGs), nodes are assigned spatial coordinates as hidden variables, and node-pairs are linked if their coordinates are closer than some threshold distance r. Hence the affinity is binary, $f(h_i,h_j) = \mathbf{1}\{\mathrm{d}_{\mathcal{X}}(h_i,h_j) \leq r\}$, with $\mathrm{d}_{\mathcal{X}} : \mathcal{X}^2 \to [0,\infty)$ denoting the geodesic distance in latent space $\mathcal{X}$. Examples of well-studied RGGs include Euclidean RGGs with periodic or nonperiodic boundary conditions [21], spherical RGGs [107], and hyperbolic RGGs (the hyperbolic model with inverse-temperature parameter $\beta = \infty$ [15]). As a primary example we consider a simple one-dimensional RGG with periodic boundary conditions: $\mathcal{X} = [0,1)$ and $\mathrm{d}_{\mathcal{X}}(h_i,h_j) = 1/2 - |1/2 - |h_i - h_j||$.

2. *Temporal RGGs*

To go from static RGGs to temporal RGGs, we incorporate coordinate-dynamics and link-resampling dynamics. We consider here jump-dynamics, each node resampling its coordinate according to the static-model density ν, with probability σ, each timestep $t \in \{2,...,T\}$ (the coordinate density follows Equation 6, with $\nu(h) = 1$ for the uniform density on the unit interval). Link-resampling happens independently for each node-pair with probability ω each timestep. Since RGGs have deterministic connectivity, link-resampling of ij at time t guarantees that $A_{ij}^{(t)} = 1$ if $\mathrm{d}_{\mathcal{X}}(h_i^{(t)},h_j^{(t)}) \leq r$ and $A_{ij}^{(t)} = 0$ otherwise. But if ij's connectivity is not resampled at time t, links may fall out-of-equilibrium with respect to coordinates. Note that we could also study temporal RGGs with walk-dynamics, with either periodic or reflecting boundary

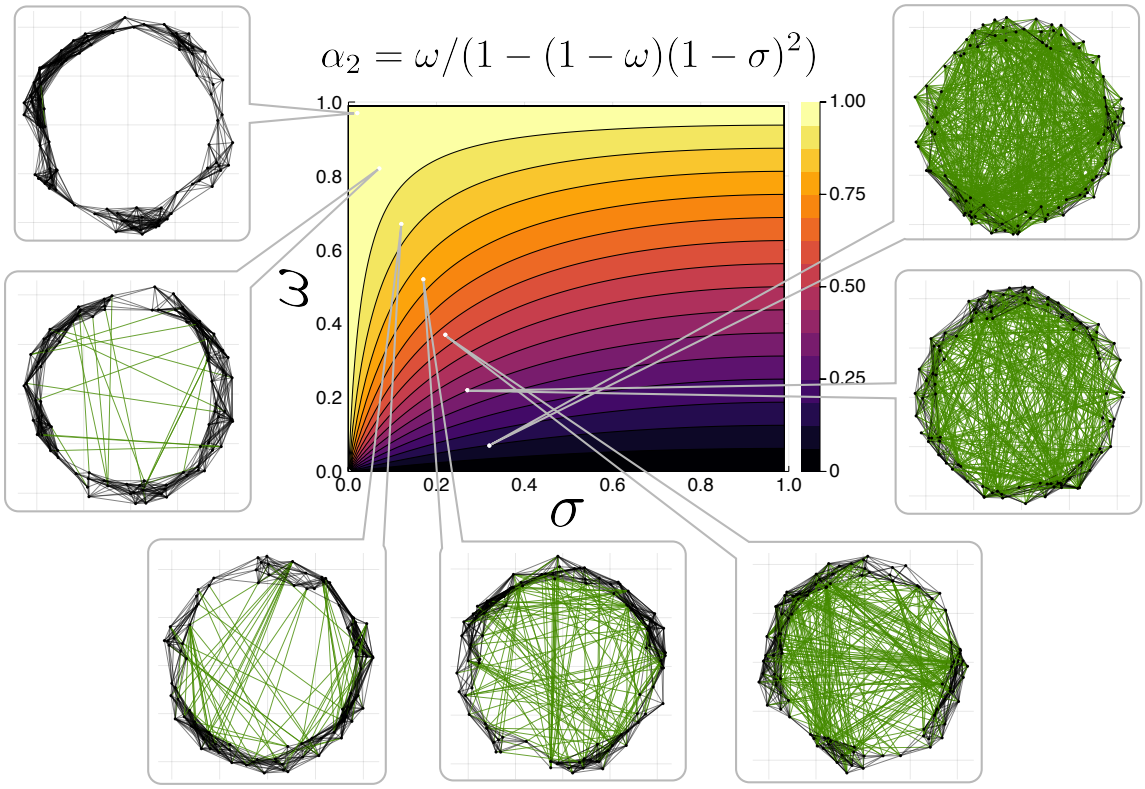

FIG. 3. **Snapshots of a temporal random geometric graphs: a geometrically-embedded network with dynamic node-coordinates and link-resampling.** Coordinates of $n = 100$ nodes are sprinkled uniformly into a 1D ring of unit circumference, and change in time via jump-dynamics (coordinate-resampling with probability σ). The affinity as a function of distance is $f(x) = \mathbf{1}\{x \leq r\}$, where $r = 0.1$ is the connection radius, disallowing long-ranged links in the *static* model. Snapshots are shown at various values of (σ, ω), with the displayed embedding having angular positions equal to 2π times spatial coordinates, and radial positions set equal to 1 plus some added random noise to aid with visualization of network connectivity amongst closeby node-pairs. **Link coloration** is according to length: black links are of distances $x \leq r$ whereas green links are of distances $x > r$. In the **central panel**, the function $\alpha_2(\sigma, \omega) \in [0, 1]$ is visualized, which encodes the level of locality in temporal RGGs (see Equation 26).

conditions; for simplicity, we study jump-dynamics here, leaving temporal RGGs with walk-dynamics for a future study.

3. *Effective connection probabilities in temporal RGGs*

We now describe the effective connection probability $\bar{f}(x)$ for RGGs between pairs of nodes for arbitrary (σ, ω). The expression for $\bar{f}(x)$ in temporal RGGs is derived in Appendix B, and the result is provided here:

$$\bar{f}(x) = \alpha_2 \mathbf{1}\{x \leq r\} + 2r(1 - \alpha_2). \tag{26}$$

The quantity $\alpha_2 = \alpha_2(\sigma, \omega)$, defined in Equation 21, directly governs the level of locality in temporal RGGs. See Figure 3 for a visualization of the function $\alpha_2(\sigma, \omega)$ and of network snapshots across a range of (σ, ω)-values. The effective connection probability $\bar{f}(x)$ has a step-like form, with connection probability $\alpha_2 + 2r(1 - \alpha_2)$ for all $x \leq r$ and $2r(1 - \alpha_2)$ for all $x > r$. The above effective connection probability agrees perfectly with the results of numerical simulations, see Figure 4.

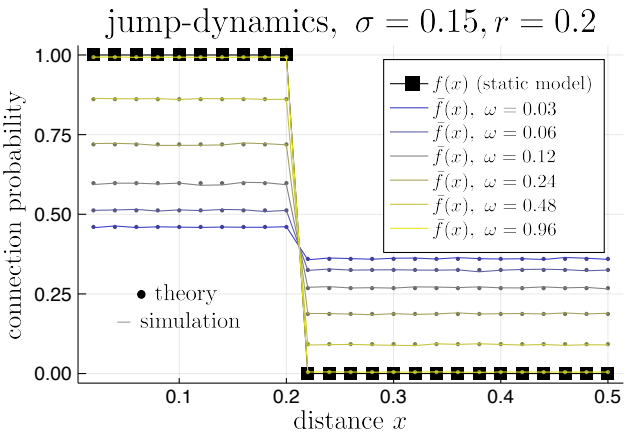

FIG. 4. **The effective connection probability, in theory and simulation, for 1D RGGs at various values of the dynamics-parameters** (σ, ω)**.** The static model affinity-function $f(x)$ is plotted with **square markers**. The **solid lines** are numerical estimates of the effective connection probability $\bar{f}(x)$ (with ω **increasing as colors change from blue to yellow**), whereas the **dotted lines** are the theoretical effective connection probability (Equation 26).

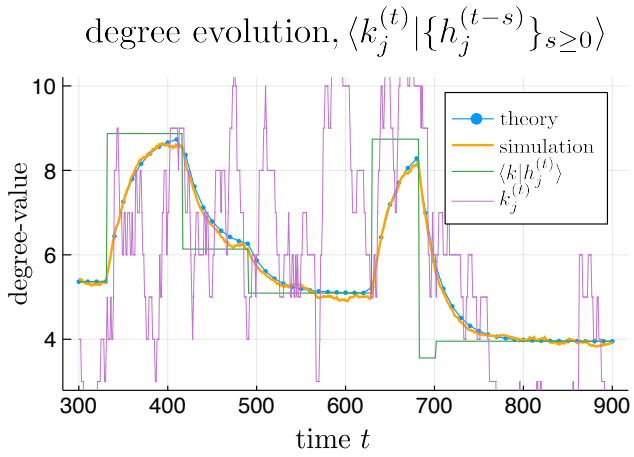

FIG. 5. **Expected degree over time of a node in a temporal hypersoft configuration model with jump-dynamics of hidden variables.** Each node's expected degree (**blue dotted curve**) equilibrates towards its current static-model expected degree (**green solid curve**), as per Equation 29. In any realization, the *actual* degree over time fluctuates (**purple curve**), but its ensemble-average (**orange solid curve**) behaves as predicted. The average was obtained by simulating 1000 realizations with $(n, \langle k \rangle, \gamma, \omega, \sigma) = (200, 8, 2.8, 0.04, 0.01)$, keeping the HV-trajectory $\{h_j^{(t)}\}_{t=1}^{T}$ of a single node j fixed across trials.

4. *Temporal RGGs discussion*

The naturally arising function $\alpha_2(\sigma, \omega) \in [0, 1]$ describes the level of locality in network snapshots (see Figure 3), and quantifies the Equilibrium Property. It interpolates between the case of RGGs ($\alpha_2(\sigma, \omega) = 1$) and ER graphs ($\alpha_2(\sigma, \omega) = 0$), resembling the structural transition of the Watts-Strogatz model [108]. In this case, all links *form* locally, and it is dynamics of *node positions* that induces the transition (alongside formation of local links at nodes' new locations); a similar phenomenon has been observed in contagion-dynamics among mobile agents [109]. Also note, in dynamic RGGs, links can exist that were not *possible* in the static model model: links of length greater than r, since the effective connection probability $\bar{f}(x)$ no longer goes completely to zero for $x > r$ (see Equation 26). This is related to phenomena observed in real-world networks: pairs of people may form friendships locally, but maintain those friendships after becoming geographically separated, resulting in the existence of long-ranged social ties that would not likely have *formed* at that distance. Likewise, the function $\bar{f}(x)$ is also *less than one* for distances $x \leq r$, allowing for *non-links* that would be impossible in the static model. That phenomenon also appears in real-world systems: instead of individuals knowing everyone in their local vicinity, non-links between closeby pairs may exist, due to them having only recently become proximate. As with the case of temporal hyper-SBMs, these examples of Qualitative Realism are *in conflict* with the Equilibrium Property. Note also that similar deviations of $\bar{f}(x)$ relative to $f(x)$ occur in THVMs arising from *soft* random geometric graphs [110–113], for example the $\mathbb{H}^2$ model (see Section V D).

C. Temporal Hypersoft Configuration Model

In this section we consider a dynamic version of hypersoft configuration models (HSCMs), which model networks with degree-heterogeneity [22].

1. *Static Hypersoft Configuration Model*

The static model we now consider is the *hypersoft configuration model* [22, 114] (HSCM), a hyperparametric version of a soft configuration model (SCM). SCMs come in several varieties such as the Chung-Lu model [115], inhomogeneous random graphs [88], and the Norros-Reittu model [116]. Node-pairs connect with A_{ij}-values being independent (typically Bernoulli or Poisson distributed), such that on average, each node has a particular degree-value. In hyperparametric SCMs, that degree-value is randomly assigned, according to some specified distribution of expected degrees. For example, one way to obtain SCMs with a degree distribution that is Pareto-mixed Poisson (with, say, power-law tail-exponent γ and expected degree $\langle k \rangle$), is for nodes $j \in [n]$ to be assigned

hidden variables $h_j \in [h_-, \infty)$ drawn from a Pareto density $\nu(h) = (\gamma-1)h_-^{\gamma-1}h^{-\gamma}$, with minimal HV-value $h_- = (\gamma-2)\langle k\rangle/(\gamma-1)$, and then for node-pairs to be connected with probability

$$f(h_i, h_j) = \frac{1}{1 + n\langle k\rangle/h_i h_j} \approx \frac{h_i h_j}{n\langle k\rangle}, \tag{27}$$

the approximation holding when $h_i h_j/n\langle k\rangle \ll 1$. The expected degree of a node i in the static model is

$$\langle k_i|h_i\rangle = (n-1)\int_{h_-}^{\infty} f(h_i, h)\nu(h)dh \approx h_i. \tag{28}$$

The *actual* degrees of nodes are sharply peaked around their expected degrees, and thus the above implies that the degree distribution itself likewise has a power-law tail with exponent γ and mean $\langle k\rangle$.

2. Temporal HSCMs

Now we consider a temporal version of HSCMs. At each timestep, each node j, with probability σ, resamples its hidden variable $h_j^{(t)}$ from the static-model HV-density ν (jump-dynamics). Then, each node-pair ij $(1 \le i < j \le n)$, with probability ω, has its indicator-variable $A_{ij}^{(t)}$ resampled from a Bernoulli of mean $f(h_i^{(t)}, h_j^{(t)})$.

In the static model, the HV-value h_j alone determines the expected degree $\langle k_j|h_j\rangle$. But in the temporal version, the quantity $h_i^{(t)}$ is time-evolving, and the expected degree dynamically trails behind the static-model expected degree, equilibrating at a geometric pace (See Figure 5):

$$\begin{aligned}
&\mathbb{E}\left[k_i^{(t)} \middle| \left\{h_i^{(t-s)}\right\}_{s\ge 0}\right] \\
&= (n-1)\omega\sum_{s\ge 0}(1-\omega)^s \int_{h_-}^{\infty} f\left(h_i^{(t-s)}, h\right)\nu(h)dh \\
&= \omega\sum_{s\ge 0}(1-\omega)^s \left\langle k_i \middle| h_i^{(t-s)}\right\rangle.
\end{aligned} \tag{29}$$

We can also average the above over all hidden-variable values at timesteps earlier than t, to obtain an *effective expected degree* that depends only on $h_j^{(t)}$. To do this, we use the probability density of $h_j^{(t-s)}$ given $h_j^{(t)}$ under jump-dynamics:

$$P_s\left(x \middle| h_j^{(t)}\right) = (1-\sigma)^s \mathbf{1}_{h_j^{(t)}}(x) + (1-(1-\sigma)^s)\,\nu(x), \tag{30}$$

Averaging Equation 29 over HVs at all timesteps $t-s$ for $s > 0$,

$$\begin{aligned}
\mathbb{E}\left[k_i^{(t)} \middle| h_i^{(t)}\right] &= \omega\sum_{s\ge 0}(1-\omega)^s \int_{h_-}^{\infty} P_s\left(x \middle| h_i^{(t)}\right)\langle k_i|x\rangle dx \\
&= \alpha_1 \left\langle k_i \middle| h_i^{(t)}\right\rangle + (1-\alpha_1)\langle k\rangle,
\end{aligned} \tag{31}$$

where $\alpha_1(\sigma,\omega) = \omega/(1-(1-\omega)(1-\sigma))$. In this case α_1 measures the level of equilibration of node-neighborhoods to their expected sizes. Having $\alpha_1 \approx 1$ indicates the quasi-static regime whereas $\alpha_1 \approx 0$ indicates an averaged-out behavior so that the expected degree of any given node is simply the expected average degree $\langle k\rangle$ of the network.

3. Effective connection probabilities in temporal HSCMs

We now discuss effective connection probabilities in HSCMs. The formula derived in Appendix A applies, but note that the affinity $f(h, h')$ (Equation 27) is a function only of the product $\psi = hh'$. Thus we can examine the *effective* connection probability as a function of ψ, denoted $\bar{f}(\psi)$. In order to calculate $\bar{f}(\psi)$ we first must compute the probability density of a product of hidden variables in past timesteps, given the value of the product at the current timestep. We then sum the expected affinity given the product, weighted by $p_s = \omega(1-\omega)^s$, over all past timesteps $s > 0$. These calculations require a variety of intermediate steps, and are described in Appendix C.

4. Temporal HSCMs discussion

Note that in HSCMs, non-equilibrium dynamics *reduces* degree-heterogeneity; nodes with large HV-values only transiently retain them. Equilibration, on the other hand, allows for a full structural expression of the nodes' internal heterogeneity. This implies that extremely heterogeneous real-world networks, if described by these models, would typically be in the quasi-static regime. We only considered jump-dynamics here (resampling of static-model expected degree-values), but we could alternatively study walk-dynamics, where nodes' HVs undergo Brownian-like motion in a way that preserves ν. This could be achieved straightforwardly as described in D, alongside reflecting boundaries as studied in Appendix E.

D. Temporal Hyperbolic Graphs

In this section we consider a temporal extension of the hyperbolic model [15] (the $\mathbb{H}^2$ model, for short), a geometry-based network model simultaneously exhibiting sparsity, clustering, small-worldness [117, 118], degree heterogeneity, community structure [119], and renormalizability [120].

1. Static $\mathbb{H}^2$ model

The $\mathbb{H}^2$ model is parameterized by a number of nodes n, average degree $\langle k\rangle$, power-law exponent γ, and inverse-

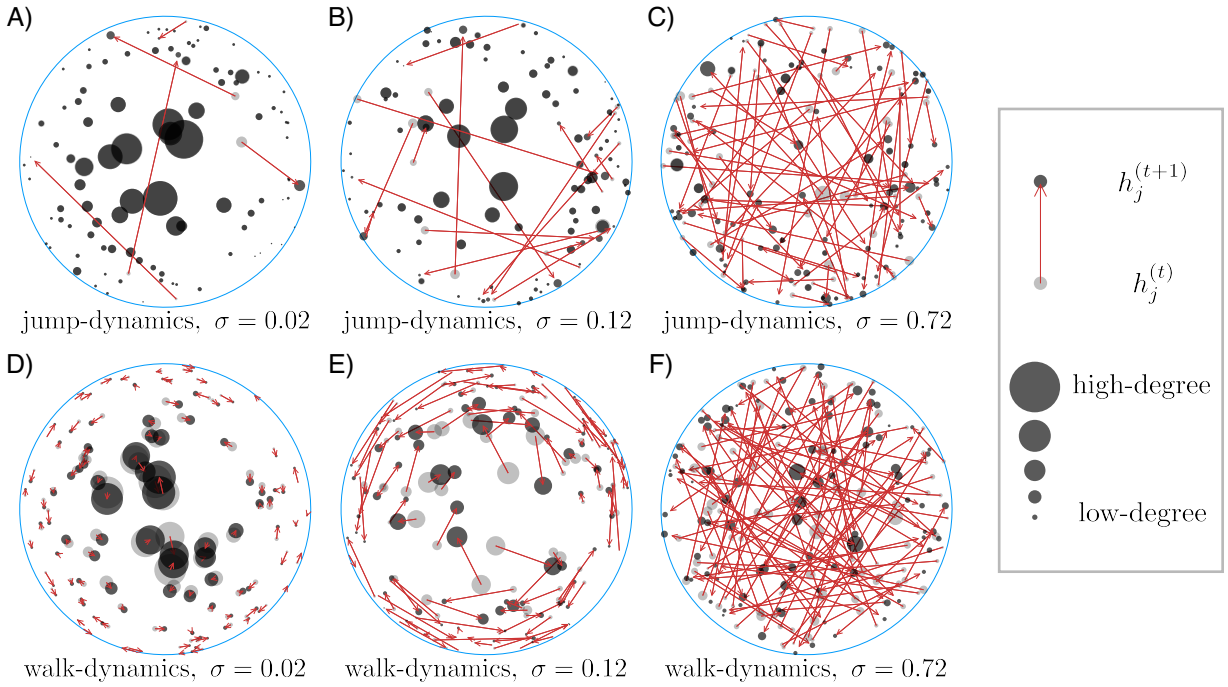

FIG. 6. **Hidden-variable dynamics of nodes in a temporal $\mathbb{H}^2$ model, at increasing values of σ, with fixed $\omega = 0.1$.** In each subplot, **node-coordinates** for 100 random nodes are shown at two adjacent timesteps, from a network with parameters $(n, \gamma, \beta, R) = (500, 2.2, 5, 8)$. Each **arrow** points from the coordinate-location of a node at a given timestep (**grey**) to the coordinate-location of the same node at the next timestep (**black**). **Subplots (A,B,C)** depict jump-dynamics (coordinate-resampling with probability σ, otherwise remaining in place), whereas **subplots (D,E,F)** depict walk-dynamics (all nodes move to neighboring locations, with mean step-length parameterized by σ). Marker sizes are proportional to node degree-values. For small σ/ω (**subplots A and D**), nodes' existing connections have arisen from approximately the present coordinates, making snapshots closely resemble the static hyperbolic model, as seen e.g. by the exhibited degree-heterogeneity. For larger σ/ω (**subplots B and E**), connections have arisen via mixtures of past and present coordinates, reducing degree-heterogeneity. For very large σ/ω (**subplots C and F**), the system behaves similarly to a temporal Erdős-Rényi network.

temperature β (which tunes the level of clustering). Hidden variables are polar coordinates, $h_j = (\theta_j, r_j)$, namely a radial coordinate $r_j \in [0, R]$ encoding the *popularity* of node j and an angular coordinate $\theta_j \in [0, 2\pi)$, encoding the *similarity* of node j to other nodes. These coordinates are sampled according to separable density $\nu(\theta, r) = \nu_{ang}(\theta)\nu_{rad}(r)$ where angles are distributed uniformly ($\nu_{ang}(\theta) = 1/2\pi$) and radii have an exponentially growing density,

$$\nu_{rad}(r) = \frac{\gamma - 1}{2} \frac{\sinh\left(\frac{\gamma-1}{2} r\right)}{\cosh\left(\frac{\gamma-1}{2} R\right) - 1}, \tag{32}$$

where $R = R(n, \langle k \rangle, \beta, \gamma)$ is selected so that the mean degree is $\langle k \rangle$. The static-model affinity of node-pair ij is a Fermi-Dirac function [121] (a sigmoid) of the hyperbolic geodesic distance x_{ij} between i and j,

$$f(h_i, h_j) = f(x_{ij}) = 1 \Big/ \left(1 + e^{(\beta/2)(x_{ij} - R)}\right), \tag{33}$$

where $x_{ij} = x_{ij}(h_i, h_j)$ is given by

$$\begin{aligned} \cosh(x_{ij}) = &\cosh(r_i)\cosh(r_j) \\ &- \sinh(r_i)\sinh(r_j)\cos(\theta_{ij}), \end{aligned} \tag{34}$$

with $\theta_{ij} = \pi - |\pi - |\theta_i - \theta_j||$. The connection probability and coordinate-density in this model result in power-law degree distributions (but could also give rise to other degree distributions if the radial coordinate-density was different), a similar feature to that exhibited by HSCMs – but also, the geometry arising from inclusion of the angular coordinate yields a large clustering coefficient and spatially localized link-structure, making this model also similar to standard RGGs. Increasing the parameter β yields more localized link-structure, approaching a step function as $\beta \to \infty$, leaving in that case an RGG (see Section V B 1) on the hyperbolic disk. As $\beta \to 0$, typical link-lengths approach the system size and the model behaves similarly to the HSCM (see Section V C 1).

2. *Temporal $\mathbb{H}^2$ model*

To temporally extend the $\mathbb{H}^2$ model, we allow coordinate dynamics so that each node j exhibits a trajectory in the hyperbolic disk, $h_j^{(t)} = (\theta_j^{(t)}, r_j^{(t)})$ for $t \in [T]$. For jump-dynamics, each node jumps to a random location according to density $\nu(\theta, r)$, with probability σ each timestep. For walk-dynamics, each node j steps

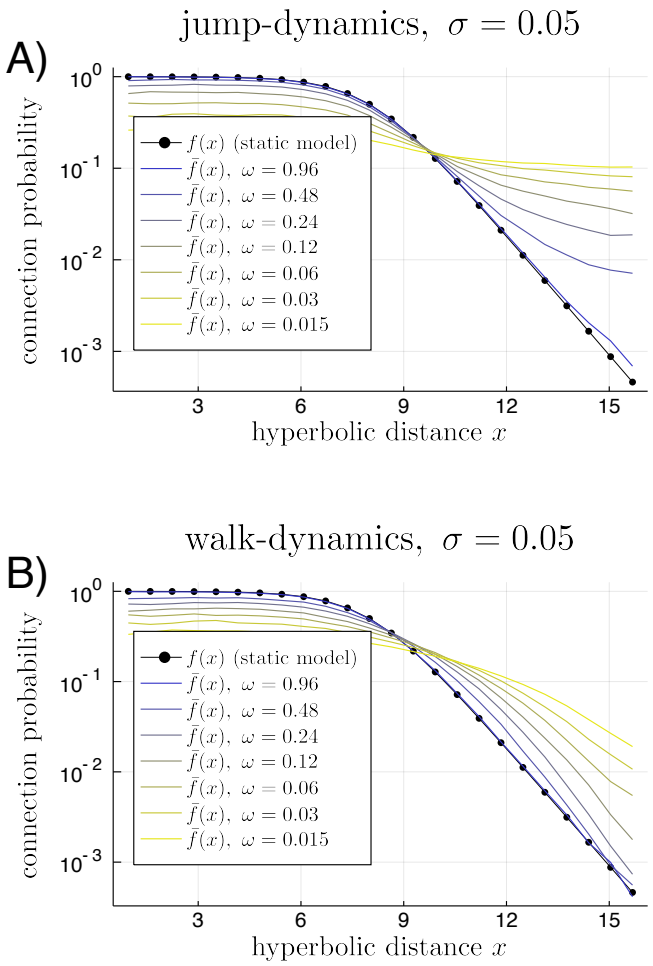

FIG. 7. **Effective connection probability function $\bar{f}(x)$ in snapshots of a temporal hyperbolic model with $(n, \gamma, \beta, R) = (500, 2.2, 5, 8)$, for various values of ω.** With slower link-resampling (smaller ω), links are increasingly allowed to dynamically stretch before being removed by link-resampling, resulting in deviations from the static-model affinity $f(x)$ (**black dotted line**). **Coloration** of the curve $\bar{f}(x)$ is from yellow to blue as ω increases. **The upper panel, A)**, shows the case of jump-dynamics of coordinates. **The lower panel, B)**, shows the case of walk-dynamics of coordinates. The choice of coordinate-dynamics is consequential in the non-equilibrium regime, despite each having the same stationary density.

to a random location $h_j^{(t+1)}$ having angular and radial coordinates adjusted to relatively closeby values, with increasingly large steps for larger σ-values; we describe the details of $\mathbb{H}^2$ walk-dynamics in Appendix F. Dynamics of nodes on the hyperbolic disk is visualized in Figure 6, for both jump-dynamics and walk-dynamics. For $\sigma \ll 1$, nodes rarely resample their coordinates (in jump-dynamics) and step to only very localized regions (in walk-dynamics). On the other hand for $\sigma \approx 1$, almost all nodes resample their coordinates at each timestep (in jump-dynamics) or move to a nearly-randomized location (in walk-dynamics). We note that many other natural and interesting choices for HV-dynamics exist, as we discuss in Section VIII and Appendix F.

3. *Effective connection probabilities in the temporal $\mathbb{H}^2$ model*

In the temporal $\mathbb{H}^2$ model considered here, the effective connection probability $\bar{f}(x)$ no longer remains in the standard Fermi-Dirac form of $f(x)$ (see Figure 7). With decreasing ω/σ, the connection probability function smooths out and extends to a longer range due to links being stretched more rapidly (for walk-dynamics), or more frequently (for jump-dynamics). This effect is more uniform and extends all the way out to long ranges for jump-dynamics, whereas it is more localized for walk-dynamics, for any given non-equilibrium value of (σ, ω).

Since the coordinates of $\mathbb{H}^2$ reflect popularity and similarity attributes, the effective connection probability and other non-equilibrium effects arising when outside of the quasi-static regime have specific interpretations. The set of current links arose from nodes having been connected at past timesteps when their previous similarity attributes were compatible (small hyperbolic distance); in real networks, such links may persist into the future even if the similarity attributes change. For instance with social networks, consider friendships on Facebook, followers on Twitter, or author collaborations: similarity between connected pairs may decrease over time, but they tend to remain connected. Likewise, it could take some time for two people that become more similar to discover one another and to connect, in an online or traditional social network.

4. *Temporal $\mathbb{H}^2$ model discussion*

Outside of the quasi-static regime, snapshots $G^{(t)}$ do not fully resemble the static $\mathbb{H}^2$ model – the Equilibrium Property is in general violated (despite the fact that *each link* was formed via the static-model connection probability corresponding to the pairwise distance at the time of that link's formation). This phenomenon results in reduced clustering because links become spread out across the space rather than being localized amongst neighboring groups of nodes. Degree-heterogeneity is also suppressed, as is the case for the temporal HSCM (see Section V C), because nodes accumulating large numbers of links due to being near the disk's center do not stay near the disk's center indefinitely. Clustering and heterogeneity arise in the *static* $\mathbb{H}^2$ model due to the correlations in links from the underlying geometry. But in the static model, all links (and non-links) arise from the *same* underlying coordinate-configuration. When coordinates are dynamical, these correlations are weaker; nodes are linked with probabilities arising as a mixture of past and

present coordinate-configurations.

VI. LINK-UPDATING IN RESPONSE TO HIDDEN-VARIABLE DYNAMICS

Finally, we describe an additional dynamical mechanism that can be incorporated to achieve the Equilibrium Property *exactly* in temporal hidden-variables models, while retaining the Persistence Property, for all values of σ and ω: links are updated *directly in response* to changes in hidden variables, rather than only through link-resampling, to keep connection probabilities up-to-date (we refer to this mechanism as link-response). In this model variant, $G^{(t+1)}$'s probability distribution depends on each of $G^{(t)}$, $H^{(t+1)}$, and $H^{(t)}$, rather than on just the former two. We illustrate the mechanism at first in the case of $\omega = 0$. Suppose node-pair ij has a link with probability $p_{ij} = f(h_i, h_j)$, and that HVs (h_i, h_j) are updated to become (h'_i, h'_j) in the next timestep. To ensure that the pair is then connected with probability $p'_{ij} = f(h'_i, h'_j)$, we selectively delete now-less-likely edges between connected pairs and selectively add now-more-likely edges between unconnected pairs. In particular:

a) If $p'_{ij} \geq p_{ij}$, then $A_{ij} = 1 \Rightarrow A'_{ij} = 1$, and $A_{ij} = 0 \Rightarrow$ add link with probability q^+_{ij},

b) If $p'_{ij} \leq p_{ij}$, then $A_{ij} = 0 \Rightarrow A'_{ij} = 0$, and $A_{ij} = 1 \Rightarrow$ remove link with probability q^-_{ij}.

The outcome needs to result in $\mathbb{P}(A'_{ij} = 1|h'_i, h'_j) = p'_{ij}$. Thus,

a) If $p'_{ij} \geq p_{ij}$, the new connection probability satisfies $p'_{ij} = p_{ij} + (1 - p_{ij})q^+_{ij}$. Hence, $q^+_{ij} = 1 - \frac{1-p'_{ij}}{1-p_{ij}}$.

b) If $p'_{ij} \leq p_{ij}$, the new connection probability satisfies $1 - p'_{ij} = p_{ij}q^-_{ij} + (1 - p_{ij})$. Hence, $q^-_{ij} = 1 - \frac{p'_{ij}}{p_{ij}}$.

Note that if $p'_{ij} = p_{ij}$, then $q^+_{ij} = q^-_{ij} = 0$; no links will form or break unless pairwise affinities change. Denoting $p^{(t)}_{ij} = f(h^{(t)}_i, h^{(t)}_j)$ for $t \in \{1, ..., T\}$, the graph transition probability given $\mathbf{H}$ becomes:

$$\mathcal{P}_G\left(G^{(t+1)}\middle|G^{(t)}, \mathbf{H}\right) = \prod_{1\leq i<j\leq n} Y_{ij}\left(A^{(t+1)}_{ij}\middle|A^{(t)}_{ij}, \mathbf{H}\right), \tag{35}$$

with $Y_{ij} : \{0, 1\} \to [0, 1]$ denoting the conditional adjacency-element probability distribution. For any $\omega \in [0, 1]$, we have:

$$Y_{ij}\left(1\middle|A^{(t)}_{ij}, \mathbf{H}\right) = \omega p^{(t+1)}_{ij} + (1-\omega)K_{ij}\left(A^{(t)}_{ij}, \mathbf{H}\right), \tag{36}$$

where $K_{ij}(A^{(t)}_{ij}, \mathbf{H})$ incorporates the link-response dynamics:

$$\begin{aligned} K_{ij}\left(A^{(t)}_{ij}, \mathbf{H}\right) =& \mathbf{1}\left\{p^{(t+1)}_{ij} \geq p^{(t)}_{ij}\right\}\left(q^+_{ij}\left(1 - A^{(t)}_{ij}\right) + A^{(t)}_{ij}\right) \\ &+ \mathbf{1}\left\{p^{(t+1)}_{ij} \leq p^{(t)}_{ij}\right\}(1 - q^-_{ij})A^{(t)}_{ij}. \end{aligned} \tag{37}$$

With the inclusion of link-response, arbitrary static hidden-variable networks can be extended to temporal settings while satisfying the Equilibrium Property exactly (See Appendix VI for a full derivation), and the Persistence Property in a tunable fashion. Allowing $\omega > 0$ does not alter the Equilibrium Property's exact validity, and it provides a more tunable level of structural persistence.

With $G^{(t)}$ indistinguishable from a static-model realization, all non-equilibrium phenomena of the types discussed in V A, V B, V C, and V D are prevented – this can either enhance or hinder Qualitative Realism, depending on the context. If a single node's HV is changed, it will need to re-evaluate connections to *all* other nodes for which affinities have changed. This could be realistic in some cases, since nodes themselves may be at the most liberty to re-evaluate their connections. In other cases, more gradual structural transitions may be preferred. This model-variant could thus serve well as a temporal null model, especially for temporal networks with snapshots well-described by an SHVM. Despite *structure* of THVMs with link-response being identical to that of SHVMs, all *dynamical* features are open for study and for comparison to real-world networks.

VII. RELATED WORK

We briefly review existing lines of research related to our study.

Several temporal network models are worth mentioning. Temporal analogs of specific static models have been considered [67–73, 122, 123], many of which preserve the Equilibrium Property. Most such models have non-dynamic node properties, yielding models related to edge-Markovian networks [99, 100, 124–126] and dynamic percolation [94–96]. The dynamic-$\mathbb{S}^1$ model [87] is a temporal extension of the static $\mathbb{S}^1$ model [15] consisting of a sequence of independent samples with HVs partially inferred from real data and partially synthetically generated; the dynamics therein resembles THVMs with $\omega = 1$ and $\sigma = 0$, but with varying average degree parameter across snapshots. Although it is common practice to extend static-model concepts to temporal settings [48–66], many models of temporal networks are instead derived from first principles [127–132], and focus primarily on inference techniques, real-world applicability [133–136], and/or the effects of temporality on spreading [86, 99].

Most relevant to THVMs are several existing works with dynamic HVs that influence link-dynamics. Several dynamic latent space models [74–77] exist, as do dy-

namic random geometric graphs [78] (the latter being continuous-time and infinite-space, with nodes sprinkled as a Poisson process [137–139] and undergoing Brownian motion [140], with links remaining up-to-date as for THVMs with $\omega = 1$). A model with both dynamic HVs and persistent links [141] was recently introduced, alongside rigorous inference techniques and applications – but not in reference to static network models. Other studies investigated spreading on dynamic RGG-like graphs [79, 109]. A few versions of dynamic SBMs are of particular relevance; in one such paper [72], the model is a case of the temporal hyper-SBM studied in Section V A with complete edge-resampling ($\omega = 1$). Another study was of a temporal hyper-SBM with $\omega < 1$ which thus exhibits both link-persistence and group-assignment-persistence [73], influencing performance of community detection algorithms and motivating the development of new ones. Another area of relevant work is the rapidly emerging area of *dynamic graph embeddings* [75, 142–154], related to the task of *inference of hidden-variable trajectories* [155].

We also note some additional works that are less-directly related to ours. Adaptive network models (for instance, SIS-dynamics [156] alongside contact-switching [23, 24]), have dynamic node-properties that evolve with time and guide network evolution, a commonality with THVMs. Networks with node-addition and node-removal [157–160] have dynamic node-properties (degree-values as opposed to hidden variables) that influence link-formation. In the fitness model of growing networks [12], static HVs and dynamic degrees both govern connection probabilities. Some static network models admit dual growing formulations [161] – analogously, if the Equlibrium Property holds, THVM snapshots can be seen as dynamically produced static-model samples. Indeed, network-rewiring and MCMC algorithms are widely used to sample static networks [162–166]; in stationarity, these can be viewed as temporal networks satisfying the Equilibrium Property, with a level of persistence tunable via the number of iterations between adjacent snapshots. Dynamic variants of the configuration model [167–169] exemplify this.

VIII. DISCUSSION

In this work we have studied temporal network models that are natural counterparts of static hidden-variables models, obtained by inclusion of a dynamic mechanism for node-characteristics (jump-dynamics or walk-dynamics) and dynamic mechanism for link-structure (link-resampling). Due to the wide generality of the static hidden-variables framework, many popular static network models can be made temporal as THVMs.

With a single source of randomness in the static model, which includes $\omega = 1$ with deterministic connectivity (Section IV B) and $\sigma = 0$ with fixed initial HVs (Section IV C), the Equilibrium Property is exactly satisfied and the Persistence Property is controllable. If, however, the static model has two layers of randomness and links are not completely refreshed each timestep ($\sigma > 0$ and $\omega < 1$), THVM snapshots are *not* in general distributed according to the static model. Rather, numerous structural deviations arise, due to links falling out-of-equilibrium with respect to hidden variables – for instance, the effective connection probability $\bar{f}(h, h')$ can substantially differ from the affinity function $f(h, h')$ (see Figures 4 and 7). Despite violating the Equilibrium Property, such models arise naturally and exhibit Qualitative Realism in interesting ways – for instance, the appearance of long-ranged links in temporal RGGs (Section V A 3) and inter-group links in temporal hyper-SBMs (Section V A 3). An exception to the non-equilibrium dynamics arises in the quasi-static regime (Section IV A) in which case the Equilibrium Property is *approximately* satisfied, due to all $A_{ij}^{(t)}$-values arising from an HV-configuration closely resembling $H^{(t)}$. A second exception arises if we add a third dynamical mechanism (Section VI), namely link-updating in *direct* response to HV-changes, which allows *exact* satisfaction of the Equilibrium Property (see Appendix G) for all (σ, ω). Both situations also lend themselves to tunable satisfaction of the Persistence Property, governed σ and ω.

An assortment of possible modifications, improvements, and extensions are worth mentioning. Although many questions are open within the present framework, altered dynamics could also be considered. For HV-dynamics, correlated motion akin to Langevin dynamics [170, 171] could provide insight into the formation and persistence of communities. Altered link-structure and link-dynamics could be considered as well: some examples include directed and/or weighted links, node-centric link-resampling dynamics [172], or pairwise-individualized resampling rates. Continuous-time formulations of THVMs could allow some theoretical simplifications; continuous time is used in studies of dynamical percolation [94, 173, 174] and edge-Markovian networks [97–101], which could each be extended to a THVM-like framework by introducing hidden variables. Our results can also inform future studies of adaptive networks [175–179]; THVMs provide a simple setting in which dynamic node-properties influence network-evolution. Understanding such settings will provide a baseline for what to expect when coevolutionary feedbacks are also present. An example of real-world links influencing node-properties is social influence, whereby acquainted pairs can become more similar over time [180, 181] – or geographically move to closer-by coordinate locations. The inclusion of interdependencies relating to dynamical processes [182, 183] can allow for more interesting dynamics and realism, but at the cost of increased model complexity.

Real-world networks have dynamic node-properties that influence dynamics of link-structure. Examples of such phenomena were set forth in Section I, ranging across a wide variety of systems and scales. One di-

rect real-world application of THVMs could be to serve as null models [65, 184] for evolving networks with dynamic node-properties [75]. Dynamic embedding methods [142–154], or generalizations of inference methods from dynamic SBMs [73], could potentially allow retrieval of $\mathbf{H}$ (and perhaps also σ, ω, and f) from an observed $\mathbf{G}$. Links of real evolving networks may not in general be fully equilibrated relative to the current set of node-characteristics, which is a dynamical behavior exhibited by THVMs *outside of the quasi-static regime*. Hence in some cases, the Equilibrium Property and Qualitative Realism may be *in conflict*, implying that caution should be used when applying static models to snapshots of evolving networks. That said, static models do in many cases accurately describe such snapshots; the internet, for example, has exhibited a clear power-law degree-tail for decades [155, 185], evidently remaining in equilibrium from the perspective of THVMs (see the discussion in V C). We expect that the present study will usefully inform general classifications of real-world networks according to the dynamics of node-properties and of how those properties influence link-dynamics.

IX. ACKNOWLEDGEMENTS

We thank B. Klein, S. Redner, M. Shrestha, L. Torres, R. Van der Hofstad, and I. Voitalov for useful discussions and suggestions. This work was supported by ARO Grant Nos. W911NF-16-1-0391 and W911NF-17-1-0491, and by NSF Grant Nos. IIS-1741355 and DMS-1800738. F.P. acknowledges support by the TV-HGGs project (OPPORTUNITY/0916/ERC-CoG/0003), funded through the Cyprus Research and Innovation Foundation.

Appendix A: Effective connection probabilities

Here we calculate effective connection probabilities for general THVMs with HVs evolving by jump-dynamics (HV-resampling with probability σ). We define the effective connection probability $\bar{f}(h,h')$ to be the probability of $A_{ij}^{(t)}=1$ given $h_i^{(t)}=h$ and $h_j^{(t)}=h'$, in the limit as $t\to\infty$. That is,

$$\bar{f}(h,h')=\lim_{t\to\infty}\mathbb{P}\left(A_{ij}^{(t)}=1\,\middle|\,h_i^{(t)}=h,h_j^{(t)}=h'\right), \quad \text{(A1)}$$

where the limit $t\to\infty$ is to wash out any initial condition. Due to the edge-resampling dynamics, the current value of $A_{ij}^{(t)}$ arose from being last resampled at some time $t-s$, with s being a random nonnegative integer having distribution $p_s=\omega(1-\omega)^s$ (where ω is the probability of link-resampling at any given timestep). The effective connection probability is given by

$$\bar{f}(h,h')=\sum_{s\geq 0}p_s\mathbb{E}\left[f\left(h_i^{(t-s)},h_j^{(t-s)}\right)\,\middle|\,h_i^{(t)}=h,h_j^{(t)}=h'\right]. \quad \text{(A2)}$$

To evaluate the above, we introduce a density $P_s(x|h)$, namely the density of $h_i^{(t-s)}$ (evaluated at x) given $h_i^{(t)}=h$. In our case, by jump-dynamics and conditioning on $h_i^{(t)}=h$, we have

$$P_s(x|h)=(1-\sigma)^s\mathbf{1}_h(x)+(1-(1-\sigma)^s)\,\nu(x), \quad \text{(A3)}$$

because h will have arisen from x after s timesteps via either (a) zero jumps having occurred, that event having probability $(1-\sigma)^s$, or via (b) *at least one* jump having occurred, in which case the density is completely randomized to $\nu(x)$. The expectation value appearing in Equation A2 is equal to

$$\begin{aligned}&\mathbb{E}\left[f\left(h_i^{(t-s)},h_j^{(t-s)}\right)\,\middle|\,h_i^{(t)}=h,h_j^{(t)}=h'\right]\\&=\int_{\mathcal{X}}\int_{\mathcal{X}}f(x,x')P_s(x|h)P_s(x'|h')dxdx',\end{aligned} \quad \text{(A4)}$$

which, using Equation A3 and integrating over (x,x'), evaluates to:

$$\begin{aligned}&(1-\sigma)^{2s}f(h,h')\\&+(1-\sigma)^s(1-(1-\sigma)^s)\left(\langle f(\cdot,h')\rangle+\langle f(h,\cdot)\rangle\right)\\&+(1-(1-\sigma)^s)^2\langle f\rangle,\end{aligned} \quad \text{(A5)}$$

where $\langle f(\cdot,h)\rangle=\langle f(h,\cdot)\rangle=\int_{\mathcal{X}}f(h,x)\nu(x)dx$ and $\langle f\rangle=\int_{\mathcal{X}^2}f(x,x')\nu(x)\nu(x')dxdx'$. Finally, plugging Equation A5 back into Equation A2, using $p_s=\omega(1-\omega)^s$ and summing the geometric series that appear ($\sum_{s\geq 0}y^s=1/(1-y)$), we obtain

$$\begin{aligned}\bar{f}(h,h')&=\alpha_2 f(h,h')\\&+(\alpha_1-\alpha_2)\left(\langle f(\cdot,h')\rangle+\langle f(h,\cdot)\rangle\right)\\&+(1-2\alpha_1+\alpha_2)\langle f\rangle,\end{aligned} \quad \text{(A6)}$$

where $\alpha_b=\alpha_b(\sigma,\omega)$ for $b\in\{1,2\}$ are given by

$$\alpha_b(\sigma,\omega)=\frac{\omega}{1-(1-\omega)(1-\sigma)^b}. \quad \text{(A7)}$$

As an aside, we note that the average degree of the network is independent of (σ,ω). This can be seen by averaging Equation A2 over h and h' and making use of $\int_{\mathcal{X}}P_s(x|h)\nu(h)dh=\nu(x)$ (which is true because $P_s(x|h)$ describes the stationary distribution, regardless of whether we consider walk-dynamics or jump-dynamics). The result is $\langle f\rangle$, regardless of σ and ω. This can be seen more directly in the case of jump-dynamics by averaging Equation A6 over h and h'.

Appendix B: Temporal RGG effective connection probability

This section contains calculations of the effective connection probability for random geometric graphs on

the unit interval with periodic boundaries and jump-dynamics. This result could be obtained from Equation A6, but we show here an alternate derivation. The effective connection probability as a function of distances is defined as the probability of two nodes *being connected* given that they are a distance $\mathrm{d}_{ij}^{(t)} = x$ apart, as $t \to \infty$:

$$\bar{f}(x) = \lim_{t\to\infty} \mathbb{P}\left(A_{ij}^{(t)} = 1 \middle| \mathrm{d}_{ij}^{(t)} = x \right). \tag{B1}$$

To calculate the above, we introduce the probability density on distances between node-pairs s timesteps prior to when the distance-value is x, denoted $P_s(y|x)$. We make use of the fact that $\mathrm{d}_{ij}^{(t)}$ can evolve in either of two ways: with probability $(1-\sigma)^2$ each timestep, *neither i nor j* jumps, and thus the density is preserved. Otherwise, one or both do jump, and their distance becomes completely randomized. The stationary density of distance x is the uniform on $[0, 1/2]$, *i.e.*, equal to 2 for all $x \in [0, 1/2]$. In a single time-advancement, jump-dynamics thus yields

$$P_1(y|x) = (1-\sigma)^2 \mathbf{1}_x(y) + 2\left(1 - (1-\sigma)^2\right). \tag{B2}$$

Iterating the above logic, $P_s(y|x)$ has two contributions: either neither node jumps at any time, or at least one node jumps at least once. Therefore,

$$P_s(y|x) = (1-\sigma)^{2s} \mathbf{1}_x(y) + 2\left(1 - (1-\sigma)^{2s}\right). \tag{B3}$$

We can compute $\bar{f}(x)$ via averaging the affinity $f(h_i, h_j) = \mathbf{1}\{\mathrm{d}_{ij}^{(t)} \le r\}$ over the distance-variable. That is,

$$\bar{f}(x) = \sum_{s\ge 0} p_s \mathbb{E}\left[\mathbf{1}\left\{ \mathrm{d}_{ij}^{(t-s)} \le r \right\} \middle| \mathrm{d}_{ij}^{(t)} = x \right], \tag{B4}$$

where the expectation term is

$$\begin{aligned}
&\mathbb{E}\left[\mathbf{1}\left\{ \mathrm{d}_{ij}^{(t-s)} \le r \right\} \middle| \mathrm{d}_{ij}^{(t)} = x \right] \\
&= \int_0^{1/2} P_s(y|x) \mathbf{1}\{y \le r\} dy \\
&= \int_0^{r} \left((1-\sigma)^{2s} \mathbf{1}_x(y) + 2\left(1 - (1-\sigma)^{2s}\right) \right) dy \\
&= (1-\sigma)^{2s} \mathbf{1}\{x \le r\} + 2r\left(1 - (1-\sigma)^{2s}\right).
\end{aligned} \tag{B5}$$

Let $s \in \{0, 1, ...\}$ be the delay since any given edge-indicator was last resampled. Recall that s has distribution $p_s = \omega(1-\omega)^s$. Then, using the above, we find

$$\begin{aligned}
\bar{f}(x) &= \omega \sum_{s\ge 0} (1-\omega)^s (1-\sigma)^{2s} \mathbf{1}\{x \le r\} \\
&\quad + \omega \sum_{s\ge 0} (1-\omega)^s 2r\left(1 - (1-\sigma)^{2s}\right) \\
&= \alpha_2 \mathbf{1}\{x \le r\} + (1-\alpha_2) 2r,
\end{aligned} \tag{B6}$$

with $\alpha_2 = \alpha_2(\sigma, \omega)$ arising from having evaluated sums of geometric series of the form $\sum_{s\ge 0}((1-\omega)(1-\sigma)^2)^s$:

$$\alpha_2(\sigma, \omega) = \frac{\omega}{1 - (1-\omega)(1-\sigma)^2}. \tag{B7}$$

Appendix C: Effective connection probability in terms of products of hidden variables

This section describes effective connection probabilities arising in temporal HSCMs, as studied in Section V C. The static-model affinity f is a function of the *product* of hidden variables, motivating study of the effective connection probability $\bar{f}$ as a function of the product of HVs as well.

Consider one-dimensional hidden variables $\{h_j\}_{j\in[n]}$ each distributed uniformly on $\mathcal{X} = [0, 1]$. This is applicable to HSCMs via the CDF-transform of arbitrary 1D probability densities: if h has density ν, then $u = F(h) = \int_{h_-}^{h} \nu(h')dh'$ is distributed uniformly on $[0, 1]$ (h_- is the minimum value of h). Denote $P_s(\phi|\psi)$ as the probability density of $\phi = h_i^{(t-s)} h_j^{(t-s)}$ for some arbitrary pair ij given that $h_i^{(t)} h_j^{(t)} = \psi$. Then,

$$\bar{f}(\psi) = \omega \sum_{s\ge 0} (1-\omega)^s \int_0^1 P_s(\phi|\psi) f(\phi) d\phi. \tag{C1}$$

For products of HVs each independently undergoing jump-dynamics, we have

$$\begin{aligned}
P_s(\phi|\psi) &= (1-\sigma)^{2s} \mathbf{1}_\psi(\phi) \\
&\quad + \left(1 - (1-\sigma)^s\right)(1-\sigma)^s p_1(\phi|\psi) \\
&\quad + \left(1 - (1-\sigma)^s\right)^2 \mu(\phi),
\end{aligned} \tag{C2}$$

with $\mu(\phi)$ denoting the product density of hidden variables and $p_1(\phi|\psi)$ the product HV-density conditioned on a single jump. Then,

$$\begin{aligned}
&\bar{f}(\psi) = \alpha f(\psi) \\
&+ \omega \sum_{s\ge 0} \left((1-\sigma)(1-\omega)\right)^s \left(1 - (1-\sigma)^s\right) \int_0^1 f(\phi) p_1(\phi|\psi) d\phi \\
&+ \omega \sum_{s\ge 0} (1-\omega)^s \left(1 - (1-\sigma)^s\right)^2 \int_0^1 f(\phi) \mu(\phi) d\phi.
\end{aligned} \tag{C3}$$

Note that $\int_0^1 f(\phi)\mu(\phi)d\phi = \langle f \rangle = \langle k \rangle / n$. Then, evaluating sums,

$$\bar{f}(\psi) = \alpha_2 f(\psi) + (\alpha_1 - \alpha_2) f_1(\psi) + (1 - 2\alpha_1 + \alpha_2)\langle f \rangle, \tag{C4}$$

with $\alpha_b = \omega / (1 - (1-\omega)(1-\sigma)^b)$, and the quantity $f_1(\psi)$ being defined as

$$f_1(\psi) = \int f(\phi) p_1(\phi|\psi) d\phi, \tag{C5}$$

where $p_1(\phi|\psi)$ is the distribution of the product of a uniform random variable and of one factor of a product, given that the value of that product is ψ. In the following, we walk through the remaining required calculations to obtain $f_1(\psi)$.

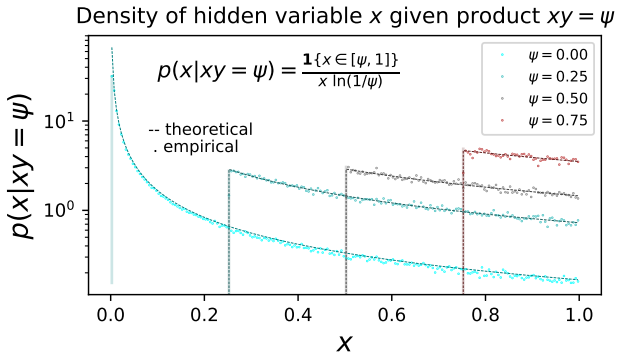

FIG. 8. The probability density of the value of one member x of a product xy conditioned on $xy = \psi$. In the absence of the conditionality, both x and y are distributed uniformly on $[0, 1]$.

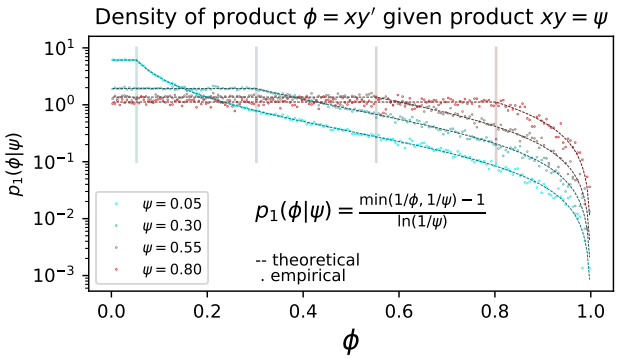

FIG. 9. The probability density of the value ϕ of the product $\phi = xy'$, where y' is uniformly sampled after having previously had random value y, and where xy was conditioned to have value $xy = \psi$. Without any conditioning, all three x, y, y' have marginal density uniform on $[0, 1]$.

1. Finding $p(x|xy = \psi)$

Suppose that x and y are sampled uniformly on $[0, 1]$. Now condition on the fact that their product, xy, takes on the particular value $xy = \psi$. Then, what is the probability density of x alone? Note first that it must reside in $[\psi, 1]$, since ψ is the product of two numbers each in the range $[0, 1]$, *i.e.*, each reducing the value of the product. Within the acceptable range, the density is obtained as follows:

$$\begin{aligned} p(x|xy=\psi) &\propto \int_0^1 \mathbf{1}_\psi(xy)dy \\ &\propto \frac{1}{x}\int_0^1 \mathbf{1}_{\psi/x}(y)dy \\ &= 1/x, \end{aligned} \tag{C6}$$

where the ratio ψ/x is guaranteed to be in the range $[0, 1]$ since $x \geq \psi$. Combining the above with the range of acceptable values of x given $xy = \psi$, we have proportionality

$$p(x|xy=\psi) = c\frac{\mathbf{1}\{x\in[\psi,1]\}}{x}, \tag{C7}$$

and c is determined by normalization:

$$\begin{aligned} 1 &= \int_0^1 p(x|xy=\psi)dx = c\int_\psi^1 \frac{dx}{x} = c\ln(1/\psi) \\ &\Rightarrow c = \frac{1}{\ln(1/\psi)}. \end{aligned} \tag{C8}$$

Therefore,

$$p(x|xy=\psi) = \frac{\mathbf{1}\{x\in[\psi,1]\}}{x\ln(1/\psi)}, \tag{C9}$$

as is confirmed numerically in Figure 8.

2. Finding $p_1(\phi|\psi)$

Now suppose that one variable, say y, undergoes a random jump (*i.e.*, is resampled) and thus becomes a new uniform variable on $[0, 1]$. The equality $xy = \psi$ no longer holds, but since it did hold prior to the jump, the variable x remains distributed according to $p(x|xy = \psi)$. Therefore the *new* product's value, which we denote by $\phi = xy'$ (where y' is the post-jump version of y), has a density $p_1(\phi|\psi)$ of the following form:

$$\begin{aligned} p_1(\phi|\psi) &= \int_0^1 \mathbf{1}\{y'\in[0,1]\}p\left(\frac{\phi}{y'}\middle| xy=\psi\right)\frac{1}{y'}dy' \\ &= \int_0^1 \frac{\mathbf{1}\{\phi/y'\in[\psi,1]\}}{(\phi/y')\ln(1/\psi)}\frac{dy'}{y'} \\ &= \frac{1}{\phi\ln(1/\psi)}\int_0^1 \mathbf{1}\{\phi/y'\in[\psi,1]\}dy'. \end{aligned} \tag{C10}$$

Continuing with a change of variables,

$$\begin{aligned} p_1(\phi|\psi) &= \frac{1}{\ln(1/\psi)}\int_0^{1/\phi} \mathbf{1}\{y'/\phi\in[1,1/\psi]\}d(y'/\phi) \\ &= \frac{\min(1/\phi,1/\psi)-1}{\ln(1/\psi)}. \end{aligned} \tag{C11}$$

The above is validated numerically in Figure 9.

3. Calculating $\bar{f}_1(\psi)$

We now average the affinity over $p_1(\phi|\psi)$, to get the contribution to the effective connection probability com-

ing from *one* hidden variable jumping. This goes as

$$\begin{aligned}\bar{f}_1(\psi) &= \int_0^1 f(\phi)p_1(\phi|\psi)d\phi \\ &= \int_0^1 f(\phi)\frac{\min(1/\phi,1/\psi)-1}{\ln(1/\psi)}d\phi \\ &= \frac{1}{\ln(1/\psi)}\left(\frac{1}{\psi}\int_0^{\psi} f(\phi)d\phi + \int_{\psi}^1 \frac{f(\phi)}{\phi}d\phi - 1\right).\end{aligned} \tag{C12}$$

Using Equation C12, we can compute $\bar{f}(\psi)$ for a given $f(\psi)$ via Equation C4.

Appendix D: Walk-Dynamics

Here we describe walk-dynamics in detail. Throughout this work, walk-dynamics in $1D$ is simulated by first mapping random variables to the unit interval (by the inverse-CDF method [186]), doing a random walk on $[0,1]$, then mapping back. For any one-dimensional probability density $\nu(x)$ where $x \in \mathbb{R}_+$, we define random variable $u(x) = F_\nu(x)$, where $F_\nu(x) = \int_0^x \nu(y)dy$. The probability density of $u(x)$ is the uniform on $[0,1]$. A random walk on $[0,1]$ is constructed via addition of uniform noise in the range $[-2\sigma, 2\sigma]$, parameterized by $\sigma \in [0,1]$. That is, after rescaling we have hidden-variable dynamics

$$\mathcal{P}_h(u'|u) = \frac{\mathbf{1}\{|u'-u| \le 2\sigma\}}{4\sigma}. \tag{D1}$$

Note that the choice of $[-2\sigma, 2\sigma]$ results in a mean jump-length equal to σ, neglecting boundary conditions; when implementing boundary conditions, one needs only to adjust the probability density $\mathcal{P}_h(u'|u)$ according to the circumstance. See Appendix E for the case of reflecting boundaries.

Drawing $h^{(1)}$ from ν, we initialize $u^{(1)} = F_\nu(h^{(1)})$ and iteratively time-advance as per the above to obtain $\{u^{(t)}\}_{t=1}^T$. We then simply transform back via $h^{(t)} = F_\nu^{-1}(u^{(t)})$, to obtain one-dimensional dynamics whose stationary distribution is ν.

In dimensions greater than 1, walk-dynamics can be simulated by first taking the multidimensional inverse-CDF transform, mapping the space $\mathcal{X}$ to a unit cube. Walk-dynamics can then be performed with whatever custom boundary conditions are required on that unit cube (boundary conditions that correspond to those of $\mathcal{X}$), and the results can then be mapped back to the original space $\mathcal{X}$. For example in the $\mathbb{H}^2$ model (Appendix F), increments of change in the angular and radial coordinates were chosen to be independent; this option was taken for simplicity, but non-independent cases would also be interesting to explore. Any transitional probability density preserving the uniform on the unit cube would fall within the same framework.

Appendix E: Walk-dynamics with reflecting boundary conditions

In this appendix we study walk-dynamics on $\mathcal{X} = [0,1]$ with *reflecting* boundary conditions under uniform noise. In particular, we show that the stationary density is uniform on $[0,1]$. In turn, that implies that arbitrary 1D dynamics with density $\nu(h)$ can be made into a random walk of this type, by mapping initial h-values to $[0,1]$ via the inverse-CDF transform, performing the reflecting random walk on $[0,1]$, then transforming the random walk trajectories back to the original space (see Appendix D).

Let $\mathcal{X} = [0,1]$ be the HV-space and denote by $x \hookleftarrow U[0,1]$ the value of a hidden variable. Then let $\hat{x} \in [-r, 1+r]$ be an intermediate variable defined as $\hat{x} = x + u$, where $u \hookleftarrow U[-r,r]$ is the uniform additive noise which we use to simulate walk-dynamics. Lastly, let $x' = Z(\hat{x})$ be the reflected variable, where the function Z encodes the reflecting boundary conditions. Note that values of x' in the ranges $[0,r]$ and $[1-r,1]$ are obtained from one of two different of values of $\hat{x}$: the case when reflected, and the case when not reflected. To transform the density of $\hat{x}$ into that of x', we write x' as a function of $\hat{z}$, as $x' = Z(\hat{x})$ and use the generalized change-of-variables formula for probability densities [187]. We denote the densities of $x, \hat{x}, x'$ as $P(x), \hat{P}(\hat{x})$, and $P'(x')$, respectively. The density of $\hat{x}$ given x is

$$\hat{P}(\hat{x}|x) = \frac{\mathbf{1}\{\hat{x} \in [x-r, x+r]\}}{2r} = \frac{\mathbf{1}\{x \in [\hat{x}-r, \hat{x}+r]\}}{2r}. \tag{E1}$$

Since x is uniform on $[0,1]$ the density of $\hat{x}$ is then

$$\begin{aligned}\hat{P}(\hat{x}) &= \int_0^1 \hat{P}(\hat{x}|x)dx \\ &= \frac{1}{2r}\int_0^1 \mathbf{1}\{x \in [\hat{x}-r, \hat{x}+r]\}dx \\ &= \frac{1}{2r}\left|[0,1] \cup [\hat{x}-r, \hat{x}+r]\right|,\end{aligned} \tag{E2}$$

or

$$\hat{P}(\hat{x}) = \frac{1}{2r}\begin{cases} \hat{x}+r, & \hat{x} < r, \\ 2r & \hat{x} \in [r, 1-r], \\ 1+r-\hat{x}, & \hat{x} > 1-r. \end{cases} \tag{E3}$$

where the $\hat{x}$-dependent coefficients of the first and third terms arise from reflections of the form $\hat{x} - (-r)$ and $1-(\hat{x}-1)$. We seek a function $Z : [-r, 1+r] \to [0,1]$ that encodes the reflection properties of the walk-dynamics. The necessary Z is given by

$$Z(\hat{x}) = \begin{cases} -\hat{x}, & \hat{x} < 0, \\ \hat{x}, & \hat{x} \in [0,1], \\ 2-\hat{x}, & \hat{x} > 1. \end{cases} \tag{E4}$$

The values of $\hat{x}$ mapping to a given value of x', namely

those making up the inverse of Z, are given by

$$\{\hat{x} : Z(\hat{x}) = x'\} = \begin{cases} \{-x', x'\}, & x' < r, \\ \{x'\}, & x' \in [r, 1-r], \\ \{x', 2-x'\}, & x' > 1-r. \end{cases} \quad \text{(E5)}$$

Let us compute the derivative of $Z(\hat{x})$, neglecting the measure-zero points of 0 and 1:

$$\frac{dZ(\hat{x})}{d\hat{x}} = \begin{cases} -1, & \hat{x} < 0, \\ 1, & \hat{x} \in (0,1), \\ -1, & \hat{x} > 1. \end{cases} \quad \text{(E6)}$$

We now transform to find the density after one step of dynamics, as

$$\begin{aligned} P'(x') &= \sum_{\hat{x}:Z(\hat{x})=x'} \left|\frac{dZ(\hat{x})}{d\hat{x}}\right|^{-1} \hat{P}(\hat{x}) \\ &= \begin{cases} \hat{P}(-x') + \hat{P}(x'), & x' < r, \\ \hat{P}(x'), & x' \in [r, 1-r], \\ \hat{P}(x') + \hat{P}(2-x'), & x' > 1-r. \end{cases} \quad \text{(E7)} \\ &= 1. \end{aligned}$$

Therefore, the stationary distribution is uniform.

Appendix F: Hyperbolic walk-dynamics

To sample $\tilde{h} = (\tilde{r}, \tilde{\theta})$, and also to sample $h_j^{(1)}$ (a coordinate from the initial timestep, *i.e.* the static $\mathbb{H}^2$ model), we first draw two independent random variables U_r and U_θ, each from the uniform distribution on $[0,1]$. These are then set equal to the cumulative density functions of ν_{rad} and ν_{ang}, evaluated at $\tilde{r}$ and $\tilde{\theta}$, respectively:

$$\begin{aligned} U_\theta &= \int_0^{\tilde{\theta}} \nu_{ang}(\theta) d\theta = \frac{\tilde{\theta}}{2\pi}, \\ U_r &= \int_0^{\tilde{r}} \nu_{rad}(r) dr = \frac{\cosh\left(\frac{\gamma-1}{2}\tilde{r}\right) - 1}{\cosh\left(\frac{\gamma-1}{2}R\right) - 1}. \end{aligned} \quad \text{(F1)}$$

From the above, we can solve to obtain $\tilde{h}$ in terms of (U_r, U_θ):

$$\begin{aligned} &\tilde{\theta} = 2\pi U_\theta, \\ &\tilde{r} = \frac{2}{\gamma-1}\cosh^{-1}\left(1 + \left(\cosh\left(\frac{\gamma-1}{2}R\right) - 1\right) U_r\right). \end{aligned} \quad \text{(F2)}$$

In the temporal setting, those initial variables are set to $U_\theta^{(1)}$ and $U_r^{(1)}$, after which we perform walk dynamics on the transformed variables to obtain $(U_\theta^{(t)}, U_r^{(t)})$ for $t \in \{2, ..., T\}$. Walk-dynamics occurs independently for the two variables, with periodic boundary conditions for angular coordinates and reflecting boundary conditions for radial coordinates.

Note that we use reflecting boundary conditions for the radial coordinate, rather than, for example, periodic boundary conditions, or reflecting boundary conditions with an associated angular reversal at any timestep that a node reflects from the origin of the radial coordinate (as would also seem like a natural choice for the disk). The reason to not incorporate such angular flipping is due to the interpretation of the angular coordinates as similarity-encoding variables [188]. From that perspective, it is more realistic to have nodes reflect off of the disk's origin and retain their similarity-coordinates, rather than to pass through the origin and reverse their similarity-coordinates.

Appendix G: Stationarity with Link-Response

In this appendix, we show that the static-model graph probability distribution is preserved via the effect of link-response as described in Section VI. Specifically, we show that

$$\int_{\mathcal{H}} \left(\sum_{G \in \mathcal{G}} \mathbb{P}(G|H) P_{H,H'}^{G \to G'}\right) \rho(H) dH = \mathbb{P}(G'|H'), \quad \text{(G1)}$$

where $P_{H^{(t)},H^{(t+1)}}^{G^{(t)} \to G^{(t+1)}} = \mathcal{P}_G(G^{(t+1)}|G^{(t)}, H^{(t+1)}, H^{(t)})$. We for now set $\omega = 0$ and later argue that link-resampling does not influence the results in question. First, we note that the transition probability given (H, H') is separable: $P_{H,H'}^{G \to G'} = \prod_{1 \le i < j \le n} P_{ij}^{A_{ij} \to A'_{ij}}$, with transition probability $P_{ij}^{\alpha \to \beta} = \mathbb{P}(A'_{ij} = \beta | A_{ij} = \alpha, h'_i, h'_j, h_i, h_j)$. Denoting $f_{ij} = f(h_i, h_j)$ and $f'_{ij} = f(h'_i, h'_j)$, we evaluate the different transition probabilities:

$$\begin{aligned} P_{ij}^{1 \to 1} &= \mathbf{1}\left\{f'_{ij} \ge f_{ij}\right\} + (1 - q_{ij}^-)\mathbf{1}\{f'_{ij} < f_{ij}\}, \\ P_{ij}^{0 \to 0} &= \mathbf{1}\left\{f'_{ij} < f_{ij}\right\} + (1 - q_{ij}^+)\mathbf{1}\{f'_{ij} \ge f_{ij}\}, \end{aligned} \quad \text{(G2)}$$

with $q_{ij}^- = 1 - f'_{ij}/f_{ij}$, $q_{ij}^+ = 1 - (1 - f'_{ij})/(1 - f_{ij})$ as defined in Section VI. The remaining probabilities are obtained by normalization:

$$\begin{aligned} P_{ij}^{1 \to 0} &= 1 - P_{ij}^{1 \to 1} = q_{ij}^- \mathbf{1}\left\{f'_{ij} < f_{ij}\right\}, \\ P_{ij}^{0 \to 1} &= 1 - P_{ij}^{0 \to 0} = q_{ij}^+ \mathbf{1}\left\{f'_{ij} \ge f_{ij}\right\}. \end{aligned} \quad \text{(G3)}$$

Noting that $P_{H,H'}^{G \to G'}$ and $\mathbb{P}(G|H)$ are both separable into a product over $ij : 1 \le i < j \le n$, we write

$$\mathbb{P}(G|H) P_{H,H'}^{G \to G'} = \prod_{1 \le i < j \le n} f_{ij}^{A_{ij}} (1 - f_{ij})^{1 - A_{ij}} P_{ij}^{A_{ij} \to A'_{ij}}. \quad \text{(G4)}$$

The sum over all graphs G of this product becomes a product over all pairs ij of a sum over $A_{ij} \in \{0, 1\}$:

$$\sum_{G \in \mathcal{G}} \prod_{1 \le i < j \le n} y(A_{ij}) = \prod_{1 \le i < j \le n} \sum_{A_{ij} \in \{0,1\}} y(A_{ij}). \quad \text{(G5)}$$

Using the above, and Equation 5, the parenthesized term in Equation G1 is equal to

$$\prod_{ij:A'_{ij}=0} \left(f_{ij}P_{ij}^{1\to 0} + (1-f_{ij})P_{ij}^{0\to 0}\right) \times \prod_{ij:A'_{ij}=1} \left(f_{ij}P_{ij}^{1\to 1} + (1-f_{ij})P_{ij}^{0\to 1}\right). \tag{G6}$$

Applying equations (G2, G3) and using the expressions for $q_{ij}^{\pm}$, as well as the facts that $\mathbf{1}\{f'_{ij} \geq f_{ij}\} + \mathbf{1}\{f'_{ij} < f_{ij}\} = 1$ and $\int_{\mathcal{H}} \rho(H)dH = 1$, Equation G1 becomes

$$\prod_{ij:A'_{ij}=1} f'_{ij} \prod_{ij:A'_{ij}=0} (1-f'_{ij}) = \mathbb{P}(G'|H'). \tag{G7}$$

The left-hand side of the above is exactly the static model's graph probability distribution given a hidden-variable configuration (see Equation 5 of the main text). Thus the static hidden-variables model is the stationary distribution of time-advancements with the link-response mechanism.

To show that these results hold even upon inclusion of the link-resampling mechanism (allowing $\omega > 0$), consider the following reasoning. Regardless of what the link-response step yielded, each node-pair undergoing link-resampling at rate ω will result in either (a) linking according to the connection probability of the newly updated hidden-variable configuration (with probability ω) or (b) linking as before ($\omega = 0$), without altering the connection probability. Given the fact that stationarity holds without link-resampling, in the latter case we also have a connection probability equal to that of the updated hidden-variable configuration.

Thus, upon inclusion of the link-response mechanism whereby both $H^{(t+1)}$ and $H^{(t)}$ impact the transition from $G^{(t)}$ to $G^{(t+1)}$, we have temporal extensions of arbitrary static hidden-variables models that *exactly* satisfy the Equilibrium property, while retaining the Persistence Property. Such a link-response mechanism may better reflect reality in cases where connectivity among nodes changes directly in response to changes in their internal characteristics.

Appendix H: Discrete hidden variables

We consider THVMs formulated with discrete hidden variables, and describe their relation to continous-HV models.

We take for example the case of SBMs, described in Section V A entirely in terms of discrete HVs, namely group-indices which are naturally thought of as discrete. We then have a set of discrete HVs $\{q_j\}_{j\in[n]}$, each distributed into a discrete set $[m] = \{1, ..., m\}$ according to a probability distribution $\varrho : [m] \to [0, 1]$, and connecting via a discrete affinity-function $f_{q,q'}$.

In a dual continuous-HV system which maps to the above-described discrete system, suppose each node j's hidden variable h_j has uniform density on $[0, 1]$, and pairwise affinities are encoded in a piecewise constant graphon function according to occupancy of points in nonoverlapping subregions $\{L_w\}_{w\in[m]} \subseteq [0, 1]^m$ such that $|L_w| = \varrho_w$ and such that

$$f(h, h') = \sum_{(w,z)\in[m]^2} f_{w,z}\mathbf{1}\{h \in L_w, h' \in L_z\}. \tag{H1}$$

Discrete node-labels can also be written directly in terms of continuous HV-values, as

$$q_i = \sum_{q\in[m]} q\mathbf{1}\{h_i \in L_q\}. \tag{H2}$$

The probability distribution ϱ thus arises from integration of the uniform density on $[0, 1]$, namely $\nu(h) = 1$, over the regions $\{L_q\}_{q\in[m]}$ corresponding to specific group-labels $q \in [m]$:

$$\varrho_q = \int_{\mathcal{X}} \nu(h)\mathbf{1}\{h \in L_q\}dh = \int_{L_q} dh = |L_q|. \tag{H3}$$

In the temporal setting, we can again relate discrete HVs to continuous ones. To reproduce the HV-resampling dynamics for temporal SBMs, we can simply have continuous HVs undergo jump-dynamics in $[0, 1]$. Jumping to a random point in $[0, 1]$ amounts to jumping into a random subset L_q with probability $\varrho_q = |L_q|$.

[1] Heeralal Janwa, Steven Massey, Julian Velev, and Bud Bhubaneswar Mishra, "On the origin of biomolecular networks," Frontiers in genetics **10**, 240 (2019).

[2] Niklas Boers, Bedartha Goswami, Aljoscha Rheinwalt, Bodo Bookhagen, Brian Hoskins, and Jürgen Kurths, "Complex networks reveal global pattern of extreme-rainfall teleconnections," Nature **566**, 373 (2019).

[3] Luciano da Fontoura Costa, Osvaldo N Oliveira Jr, Gonzalo Travieso, Francisco Aparecido Rodrigues, Paulino Ribeiro Villas Boas, Lucas Antiqueira, Matheus Palhares Viana, and Luis Enrique Correa Rocha, "Analyzing and modeling real-world phenomena with complex networks: a survey of applications," Advances in Physics **60**, 329–412 (2011).

[4] Luis EC Rocha, Fredrik Liljeros, and Petter Holme, "Information dynamics shape the sexual networks of internet-mediated prostitution," Proceedings of the National Academy of Sciences **107**, 5706–5711 (2010).

[5] Geoffrey B West, James H Brown, and Brian J Enquist, "A general model for the origin of allometric scaling laws in biology," Science **276**, 122–126 (1997).

[6] Romualdo Pastor-Satorras and Alessandro Vespignani, *Evolution and structure of the Internet: A statistical physics approach* (Cambridge University Press, 2004).

[7] Muhua Zheng, Antoine Allard, Patric Hagmann, Yasser Alemán-Gómez, and M Ángeles Serrano, "Geometric renormalization unravels self-similarity of the multiscale human connectome," Proceedings of the National Academy of Sciences **117**, 20244–20253 (2020).

[8] Giulio Cimini, Tiziano Squartini, Fabio Saracco, Diego Garlaschelli, Andrea Gabrielli, and Guido Caldarelli, "The statistical physics of real-world networks," Nature Reviews Physics **1**, 58–71 (2019).

[9] Hyunju Kim, Harrison B Smith, Cole Mathis, Jason Raymond, and Sara I Walker, "Universal scaling across biochemical networks on earth," Science advances **5**, eaau0149 (2019).

[10] Paul L Krapivsky and Sidney Redner, "A statistical physics perspective on web growth," Computer Networks **39**, 261–276 (2002).

[11] Albert-László Barabási and Réka Albert, "Emergence of scaling in random networks," science **286**, 509–512 (1999).

[12] Ginestra Bianconi and A-L Barabási, "Competition and multiscaling in evolving networks," EPL (Europhysics Letters) **54**, 436 (2001).

[13] Guido Caldarelli, Andrea Capocci, Paolo De Los Rios, and Miguel A Munoz, "Scale-free networks from varying vertex intrinsic fitness," Physical review letters **89**, 258702 (2002).

[14] Marc Barthelemy, *Morphogenesis of spatial networks* (Springer, 2018).

[15] Dmitri Krioukov, Fragkiskos Papadopoulos, Maksim Kitsak, Amin Vahdat, and Marián Boguná, "Hyperbolic geometry of complex networks," Physical Review E **82**, 036106 (2010).

[16] M Ángeles Serrano, Marián Boguná, and Francesc Sagués, "Uncovering the hidden geometry behind metabolic networks," Molecular biosystems **8**, 843–850 (2012).

[17] Maksim Kitsak, Fragkiskos Papadopoulos, and Dmitri Krioukov, "Latent geometry of bipartite networks," Physical Review E **95**, 032309 (2017).

[18] Marián Boguná and Romualdo Pastor-Satorras, "Class of correlated random networks with hidden variables," Physical Review E **68**, 036112 (2003).

[19] Mark Newman, *Networks* (Oxford university press, 2018).

[20] Brian Karrer and Mark EJ Newman, "Stochastic blockmodels and community structure in networks," Physical review E **83**, 016107 (2011).

[21] Mathew Penrose *et al.*, *Random geometric graphs*, Vol. 5 (Oxford university press, 2003).

[22] Pim van der Hoorn, Gabor Lippner, and Dmitri Krioukov, "Sparse maximum-entropy random graphs with a given power-law degree distribution," Journal of Statistical Physics **173**, 806–844 (2018).

[23] Sebastián Risau-Gusmán and Damián H Zanette, "Contact switching as a control strategy for epidemic outbreaks," Journal of theoretical biology **257**, 52–60 (2009).

[24] Suwakan Piankoranee and Surachate Limkumnerd, "Effects of global and local rewiring on sis epidemic adaptive networks," in *Journal of Physics: Conference Series*, Vol. 1144 (IOP Publishing, 2018) p. 012080.

[25] Cristián Huepe, Gerd Zschaler, Anne-Ly Do, and Thilo Gross, "Adaptive-network models of swarm dynamics," New Journal of Physics **13**, 073022 (2011).

[26] Vincent Marceau, Pierre-André Noël, Laurent Hébert-Dufresne, Antoine Allard, and Louis J Dubé, "Adaptive networks: Coevolution of disease and topology," Physical Review E **82**, 036116 (2010).

[27] Guven Demirel, Federico Vazquez, GA Böhme, and Thilo Gross, "Moment-closure approximations for discrete adaptive networks," Physica D: Nonlinear Phenomena **267**, 68–80 (2014).

[28] Thilo Gross and Hiroki Sayama, "Adaptive networks," in *Adaptive networks* (Springer, 2009) pp. 1–8.

[29] I Barry Crabtree and Stuart J Soltysiak, "Identifying and tracking changing interests," International Journal on Digital Libraries **2**, 38–53 (1998).

[30] Ben B Chapman, Christer Brönmark, Jan-Åke Nilsson, and Lars-Anders Hansson, "The ecology and evolution of partial migration," Oikos **120**, 1764–1775 (2011).

[31] Yannis Vardanis, Raymond HG Klaassen, Roine Strandberg, and Thomas Alerstam, "Individuality in bird migration: routes and timing," Biology letters **7**, 502–505 (2011).

[32] Sonia Altizer, Rebecca Bartel, and Barbara A Han, "Animal migration and infectious disease risk," science **331**, 296–302 (2011).

[33] Martin Pfeffer and Gerhard Dobler, "Emergence of zoonotic arboviruses by animal trade and migration," Parasites & vectors **3**, 35 (2010).

[34] Andrew M Hein, Chen Hou, and James F Gillooly, "Energetic and biomechanical constraints on animal migration distance," Ecology letters **15**, 104–110 (2012).

[35] Scott P Carroll, Andrew P Hendry, David N Reznick, and Charles W Fox, "Evolution on ecological timescales," Functional Ecology **21**, 387–393 (2007).

[36] Torsten Held, Armita Nourmohammad, and Michael Lässig, "Adaptive evolution of molecular phenotypes," Journal of Statistical Mechanics: Theory and Experiment **2014**, P09029 (2014).

[37] Henk W Volberda and Arie Y Lewin, "Co-evolutionary dynamics within and between firms: From evolution to co-evolution," Journal of management studies **40**, 2111–2136 (2003).

[38] Michael Stoica and Minet Schindehutte, "Understanding adaptation in small firms: Links to culture and performance," Journal of Developmental Entrepreneurship **4**, 1 (1999).

[39] Kenneth M Johnson, "Demographic trends in rural and small town america," (2006), 10.34051/p/2020.6.

[40] Dowell Myers, "Demographic dynamism and metropolitan change: Comparing los angeles, new york, chicago, and washington, dc," Housing Policy Debate **10**, 919–954 (1999).

[41] Juste Raimbault, "Modeling the co-evolution of cities and networks," arXiv preprint arXiv:1804.09430 (2018).

[42] Siobhan G Kuhar, Lei Feng, Susana Vidan, M Elizabeth Ross, Mary E Hatten, and Nathaniel Heintz, "Changing patterns of gene expression define four stages of cerebellar granule neuron differentiation," Development **117**, 97–104 (1993).

[43] Matthew A McCormack, Kenneth M Rosen, Lydia Villa-Komaroff, and George D Mower, "Changes in immediate early gene expression during postnatal development of cat cortex and cerebellum," Molecular brain research **12**, 215–223 (1992).

[44] Mohammad Moradi Dalvand, Seyed Bahram Zahir Azami, and Hadi Tarimoradi, "Long-term load forecasting of iranian power grid using fuzzy and artificial neural networks," in *2008 43rd International Universities Power Engineering Conference* (IEEE, 2008) pp. 1–4.

[45] Matteo De Felice, Andrea Alessandri, and Paolo M Ruti, "Electricity demand forecasting over italy: Potential benefits using numerical weather prediction models," Electric Power Systems Research **104**, 71–79 (2013).

[46] Natalia Pasichnyk, Mykola Dyvak, and Roman Pasichnyk, "Mathematical modeling of website quality characteristics in dynamics," in *Journal of Applied Computer Science*, Vol. 22 (Technical University Press, 2014) pp. 171–183.

[47] Sandra J Bean, "Emerging and continuing trends in vaccine opposition website content," Vaccine **29**, 1874–1880 (2011).

[48] Vincenzo Nicosia, John Tang, Cecilia Mascolo, Mirco Musolesi, Giovanni Russo, and Vito Latora, "Graph metrics for temporal networks," in *Temporal networks* (Springer, 2013) pp. 15–40.

[49] Elisenda Ortiz, Michele Starnini, and M Ángeles Serrano, "Navigability of temporal networks in hyperbolic space," Scientific reports **7**, 15054 (2017).

[50] Dane Taylor, Sean A Myers, Aaron Clauset, Mason A Porter, and Peter J Mucha, "Eigenvector-based centrality measures for temporal networks," Multiscale Modeling & Simulation **15**, 537–574 (2017).

[51] Hyoungshick Kim and Ross Anderson, "Temporal node centrality in complex networks," Physical Review E **85**, 026107 (2012).

[52] Raj Kumar Pan and Jari Saramäki, "Path lengths, correlations, and centrality in temporal networks," Physical Review E **84**, 016105 (2011).

[53] Aming Li, Sean P Cornelius, Y-Y Liu, Long Wang, and A-L Barabási, "The fundamental advantages of temporal networks," Science **358**, 1042–1046 (2017).

[54] Suyu Liu, Nicola Perra, Márton Karsai, and Alessandro Vespignani, "Controlling contagion processes in activity driven networks," Physical review letters **112**, 118702 (2014).

[55] Nicola Perra, Andrea Baronchelli, Delia Mocanu, Bruno Gonçalves, Romualdo Pastor-Satorras, and Alessandro Vespignani, "Random walks and search in time-varying networks," Physical review letters **109**, 238701 (2012).

[56] Ashwin Paranjape, Austin R Benson, and Jure Leskovec, "Motifs in temporal networks," in *Proceedings of the Tenth ACM International Conference on Web Search and Data Mining* (ACM, 2017) pp. 601–610.

[57] Petter Holme, "Temporal network structures controlling disease spreading," Physical Review E **94**, 022305 (2016).

[58] Quan-Hui Liu, Xinyue Xiong, Qian Zhang, and Nicola Perra, "Epidemic spreading on time-varying multiplex networks," Physical Review E **98**, 062303 (2018).

[59] Matthieu Nadini, Kaiyuan Sun, Enrico Ubaldi, Michele Starnini, Alessandro Rizzo, and Nicola Perra, "Epidemic spreading in modular time-varying networks," Scientific reports **8**, 2352 (2018).

[60] Naoki Masuda and Petter Holme, *Temporal network epidemiology* (Springer, 2017).

[61] Kaiyuan Sun, Andrea Baronchelli, and Nicola Perra, "Contrasting effects of strong ties on sir and sis processes in temporal networks," The European Physical Journal B **88**, 326 (2015).

[62] Dandan Li, Dun Han, Jing Ma, Mei Sun, Lixin Tian, Timothy Khouw, and H Eugene Stanley, "Opinion dynamics in activity-driven networks," EPL (Europhysics Letters) **120**, 28002 (2018).

[63] Daniel M Dunlavy, Tamara G Kolda, and Evrim Acar, "Temporal link prediction using matrix and tensor factorizations," ACM Transactions on Knowledge Discovery from Data (TKDD) **5**, 10 (2011).

[64] Yugchhaya Dhote, Nishchol Mishra, and Sanjeev Sharma, "Survey and analysis of temporal link prediction in online social networks," in *2013 International Conference on Advances in Computing, Communications and Informatics (ICACCI)* (IEEE, 2013) pp. 1178–1183.

[65] Marta Sarzynska, Elizabeth A Leicht, Gerardo Chowell, and Mason A Porter, "Null models for community detection in spatially embedded, temporal networks," Journal of Complex Networks **4**, 363–406 (2016).

[66] Laetitia Gauvin, André Panisson, and Ciro Cattuto, "Detecting the community structure and activity patterns of temporal networks: a non-negative tensor factorization approach," PloS one **9**, e86028 (2014).

[67] Tiago P Peixoto and Martin Rosvall, "Modelling sequences and temporal networks with dynamic community structures," Nature communications **8**, 582 (2017).

[68] Kevin S Xu and Alfred O Hero, "Dynamic stochastic blockmodels for time-evolving social networks," IEEE Journal of Selected Topics in Signal Processing **8**, 552–562 (2014).

[69] Kevin Xu, "Stochastic block transition models for dynamic networks," in *Artificial Intelligence and Statistics* (2015) pp. 1079–1087.

[70] Catherine Matias and Vincent Miele, "Statistical clustering of temporal networks through a dynamic stochastic block model," Journal of the Royal Statistical Society: Series B (Statistical Methodology) **79**, 1119–1141 (2017).

[71] Marianna Pensky, Teng Zhang, *et al.*, "Spectral clustering in the dynamic stochastic block model," Electronic Journal of Statistics **13**, 678–709 (2019).

[72] Amir Ghasemian, Pan Zhang, Aaron Clauset, Cristopher Moore, and Leto Peel, "Detectability thresholds and optimal algorithms for community structure in dynamic networks," Physical Review X **6**, 031005 (2016).

[73] Paolo Barucca, Fabrizio Lillo, Piero Mazzarisi, and Daniele Tantari, "Disentangling group and link persistence in dynamic stochastic block models," Journal of Statistical Mechanics: Theory and Experiment **2018**, 123407 (2018).

[74] Daniel K Sewell and Yuguo Chen, "Latent space models for dynamic networks with weighted edges," Social Networks **44**, 105–116 (2016).

[75] Bomin Kim, Kevin H Lee, Lingzhou Xue, and Xiaoyue Niu, "A review of dynamic network models with latent variables," Statistics surveys **12**, 105 (2018).

[76] Purnamrita Sarkar, Sajid M Siddiqi, and Geogrey J Gordon, "A latent space approach to dynamic embedding of co-occurrence data," in *Artificial Intelligence and Statistics* (2007) pp. 420–427.

[77] Purnamrita Sarkar and Andrew W Moore, "Dynamic

social network analysis using latent space models," in *Advances in Neural Information Processing Systems* (2006) pp. 1145–1152.
[78] Yuval Peres, Alistair Sinclair, Perla Sousi, and Alexandre Stauffer, "Mobile geometric graphs: Detection, coverage and percolation," Probability Theory and Related Fields **156**, 273–305 (2013).
[79] Andrea Clementi and Riccardo Silvestri, "Parsimonious flooding in geometric random-walks," Journal of Computer and System Sciences **81**, 219–233 (2015).
[80] Harrison Hartle, Brennan Klein, Stefan McCabe, Alexander Daniels, Guillaume St-Onge, Charles Murphy, and Laurent Hébert-Dufresne, "Network comparison and the within-ensemble graph distance," Proceedings of the Royal Society A **476**, 20190744 (2020).
[81] James R Norris, *Markov chains*, 2 (Cambridge university press, 1998).
[82] Ehrhard Behrends, *Introduction to Markov chains*, Vol. 228 (Springer, 2000).
[83] Ginestra Bianconi, *Multilayer networks: structure and function* (Oxford university press, 2018).
[84] Manlio De Domenico, Albert Solé-Ribalta, Emanuele Cozzo, Mikko Kivelä, Yamir Moreno, Mason A Porter, Sergio Gómez, and Alex Arenas, "Mathematical formulation of multilayer networks," Physical Review X **3**, 041022 (2013).
[85] Peter T Landsberg, "Foundations of thermodynamics," Reviews of modern physics **28**, 363 (1956).
[86] Nicola Perra, Bruno Goncalves, Romualdo Pastor-Satorras, and Alessandro Vespignani, "Activity driven modeling of time varying networks," Scientific Reports **2**, 469 (2012).
[87] Fragkiskos Papadopoulos and Marco Antonio Rodríguez Flores, "Latent geometry and dynamics of proximity networks," Physical Review E **100**, 052313 (2019).
[88] Béla Bollobás, Svante Janson, and Oliver Riordan, "The phase transition in inhomogeneous random graphs," Random Structures & Algorithms **31**, 3–122 (2007).
[89] Roberto Imbuzeiro Oliveira, "Concentration of the adjacency matrix and of the laplacian in random graphs with independent edges," arXiv preprint arXiv:0911.0600 (2009).
[90] Linyuan Lu and Xing Peng, "Spectra of edge-independent random graphs," arXiv preprint arXiv:1204.6207 (2012).
[91] Paul Erdos and Alfred Renyi, "On random graphs i," Publ. math. debrecen **6**, 18 (1959).
[92] Carolyn J Anderson, Stanley Wasserman, and Katherine Faust, "Building stochastic blockmodels," Social networks **14**, 137–161 (1992).
[93] Richard W Hamming, "Error detecting and error correcting codes," The Bell system technical journal **29**, 147–160 (1950).
[94] Jeffrey E Steif, "A survey of dynamical percolation," in *Fractal geometry and stochastics IV* (Springer, 2009) pp. 145–174.
[95] Yuval Peres and Jeffrey E Steif, "The number of infinite clusters in dynamical percolation," Probability theory and related fields **111**, 141–165 (1998).
[96] Davar Khoshnevisan, "Dynamical percolation on general trees," Probability theory and related fields **140**, 169–193 (2008).
[97] Matthew I Roberts, Batı Şengül, *et al.*, "Exceptional times of the critical dynamical erdős–rényi graph," The Annals of Applied Probability **28**, 2275–2308 (2018).
[98] Raphaël Rossignol, "Scaling limit of dynamical percolation on critical erdös-rényi random graphs," arXiv preprint arXiv:1710.09101 (2020).
[99] Andrea EF Clementi, Claudio Macci, Angelo Monti, Francesco Pasquale, and Riccardo Silvestri, "Flooding time of edge-markovian evolving graphs," SIAM journal on discrete mathematics **24**, 1694–1712 (2010).
[100] John Whitbeck, Vania Conan, and Marcelo Dias de Amorim, "Performance of opportunistic epidemic routing on edge-markovian dynamic graphs," IEEE Transactions on communications **59**, 1259–1263 (2011).
[101] Aurelie Faure de Pebeyre, Fabien Tarissan, and Julien Sopena, "On the relevance of the edge-markovian evolving graph model for real mobile networks," in *2013 IFIP Wireless Days (WD)* (IEEE, 2013) pp. 1–6.
[102] Tiago P Peixoto, "Entropy of stochastic blockmodel ensembles," Physical Review E **85**, 056122 (2012).
[103] Tiago P Peixoto, "Nonparametric bayesian inference of the microcanonical stochastic block model," Physical Review E **95**, 012317 (2017).
[104] Stephen G Kobourov, "Spring embedders and force directed graph drawing algorithms," arXiv preprint arXiv:1201.3011 (2012).
[105] Bo Söderberg, "Random graphs with hidden color," Physical Review E **68**, 015102 (2003).
[106] Bo Söderberg, "General formalism for inhomogeneous random graphs," Physical review E **66**, 066121 (2002).
[107] Alfonso Allen-Perkins, "Random spherical graphs," Physical Review E **98**, 032310 (2018).
[108] Duncan J Watts and Steven H Strogatz, "Collective dynamics of small-worldnetworks," nature **393**, 440–442 (1998).
[109] Arturo Buscarino, Luigi Fortuna, Mattia Frasca, and Vito Latora, "Disease spreading in populations of moving agents," EPL (Europhysics Letters) **82**, 38002 (2008).
[110] Mathew D Penrose *et al.*, "Connectivity of soft random geometric graphs," The Annals of Applied Probability **26**, 986–1028 (2016).
[111] Michael Wilsher, Carl P Dettmann, and Ayalvadi Ganesh, "Connectivity in one-dimensional soft random geometric graphs," arXiv preprint arXiv:2007.06301 (2020).
[112] Marcus Kaiser and Claus C Hilgetag, "Spatial growth of real-world networks," Physical Review E **69**, 036103 (2004).
[113] Carl P Dettmann and Orestis Georgiou, "Random geometric graphs with general connection functions," Physical Review E **93**, 032313 (2016).
[114] Ivan Voitalov, Pim van der Hoorn, Maksim Kitsak, Fragkiskos Papadopoulos, and Dmitri Krioukov, "Weighted hypersoft configuration model," Physical Review Research **2**, 043157 (2020).
[115] Fan Chung and Linyuan Lu, "Connected components in random graphs with given expected degree sequences," Annals of combinatorics **6**, 125–145 (2002).
[116] Ilkka Norros and Hannu Reittu, "On a conditionally poissonian graph process," Advances in Applied Probability **38**, 59–75 (2006).
[117] Karl Bringmann, Ralph Keusch, and Johannes Lengler, "Average distance in a general class of scale-free networks with underlying geometry," arXiv preprint

arXiv:1602.05712 (2016).
[118] Tobias Friedrich and Anton Krohmer, "On the diameter of hyperbolic random graphs," SIAM Journal on Discrete Mathematics **32**, 1314–1334 (2018).
[119] Ali Faqeeh, Saeed Osat, and Filippo Radicchi, "Characterizing the analogy between hyperbolic embedding and community structure of complex networks," Physical review letters **121**, 098301 (2018).
[120] Guillermo García-Pérez, Marián Boguñá, and M Ángeles Serrano, "Multiscale unfolding of real networks by geometric renormalization," Nature Physics **14**, 583–589 (2018).
[121] Mehran Kardar, *Statistical physics of particles* (Cambridge University Press, 2007).
[122] Xiao Zhang, Cristopher Moore, and Mark EJ Newman, "Random graph models for dynamic networks," The European Physical Journal B **90**, 200 (2017).
[123] Michel Mandjes, Nicos Starreveld, René Bekker, and Peter Spreij, "Dynamic erdős-rényi graphs," in *Computing and Software Science* (Springer, 2019) pp. 123–140.
[124] Andrea EF Clementi, Francesco Pasquale, Angelo Monti, and Riccardo Silvestri, "Information spreading in stationary markovian evolving graphs," in *2009 IEEE International Symposium on Parallel & Distributed Processing* (IEEE, 2009) pp. 1–12.
[125] Ruijie Du, Hanxing Wang, and Yunbin Fu, "Continuous-time independent edge-markovian random graph process," Chinese Annals of Mathematics, Series B **37**, 73–82 (2016).
[126] Ioannis Lamprou, Russell Martin, and Paul Spirakis, "Cover time in edge-uniform stochastically-evolving graphs," Algorithms **11**, 149 (2018).
[127] Lorenzo Zino, Alessandro Rizzo, and Maurizio Porfiri, "Continuous-time discrete-distribution theory for activity-driven networks," Physical review letters **117**, 228–302 (2016).
[128] Iacopo Pozzana, Kaiyuan Sun, and Nicola Perra, "Epidemic spreading on activity-driven networks with attractiveness," Physical Review E **96**, 042310 (2017).
[129] Angélica Sousa da Mata and Romualdo Pastor-Satorras, "Slow relaxation dynamics and aging in random walks on activity driven temporal networks," The European Physical Journal B **88**, 12 (2015).
[130] Laura Alessandretti, Kaiyuan Sun, Andrea Baronchelli, and Nicola Perra, "Random walks on activity-driven networks with attractiveness," Physical Review E **95**, 052318 (2017).
[131] Alessandro Rizzo and Maurizio Porfiri, "Innovation diffusion on time-varying activity driven networks," The European Physical Journal B **89**, 20 (2016).
[132] Michele Starnini and Romualdo Pastor-Satorras, "Temporal percolation in activity-driven networks," Physical Review E **89**, 032807 (2014).
[133] Adrian Silvescu and Vasant Honavar, "Temporal boolean network models of genetic networks and their inference from gene expression time series," Complex systems **13**, 61–78 (2001).
[134] Sophie Lebre, Jennifer Becq, Frederic Devaux, Michael PH Stumpf, and Gaelle Lelandais, "Statistical inference of the time-varying structure of gene-regulation networks," BMC systems biology **4**, 130 (2010).
[135] Steve Hanneke, Wenjie Fu, Eric P Xing, *et al.*, "Discrete temporal models of social networks," Electronic Journal of Statistics **4**, 585–605 (2010).
[136] Andrew Mellor, "Event graphs: Advances and applications of second-order time-unfolded temporal network models," Advances in Complex Systems **22**, 1950006 (2019).
[137] Roger E Miles, "On the homogeneous planar poisson point process," Mathematical Biosciences **6**, 85–127 (1970).
[138] Jesper Møller and Rasmus P Waagepetersen, "Modern statistics for spatial point processes," Scandinavian Journal of Statistics **34**, 643–684 (2007).
[139] Matthias Reitzner, "Poisson point processes: large deviation inequalities for the convex distance," (2013), 10.1214/ecp.v18-2851.
[140] SR Srinivasa Varadhan, *Stochastic processes*, Vol. 16 (American Mathematical Soc., 2007).
[141] P Mazzarisi, P Barucca, F Lillo, and D Tantari, "A dynamic network model with persistent links and node-specific latent variables, with an application to the interbank market," European Journal of Operational Research **281**, 50–65 (2020).
[142] Ranran Bian, Yun Sing Koh, Gillian Dobbie, and Anna Divoli, "Network embedding and change modeling in dynamic heterogeneous networks," in *Proceedings of the 42nd International ACM SIGIR Conference on Research and Development in Information Retrieval* (2019) pp. 861–864.
[143] Palash Goyal, Sujit Rokka Chhetri, Ninareh Mehrabi, Emilio Ferrara, and Arquimedes Canedo, "Dynamicgem: A library for dynamic graph embedding methods," arXiv preprint arXiv:1811.10734 (2018).
[144] Yuanfu Lu, Xiao Wang, Chuan Shi, Philip S Yu, and Yanfang Ye, "Temporal network embedding with micro- and macro-dynamics," in *Proceedings of the 28th ACM International Conference on Information and Knowledge Management* (2019) pp. 469–478.
[145] Yu Xie, Chunyi Li, Bin Yu, Chen Zhang, and Zhouhua Tang, "A survey on dynamic network embedding," arXiv preprint arXiv:2006.08093 (2020).
[146] Mounir Haddad, Cécile Bothorel, Philippe Lenca, and Dominique Bedart, "Temporalnode2vec: Temporal node embedding in temporal networks," in *International Conference on Complex Networks and Their Applications* (Springer, 2019) pp. 891–902.
[147] Di Jin, Sungchul Kim, Ryan A Rossi, and Danai Koutra, "From static to dynamic node embeddings," arXiv preprint arXiv:2009.10017 (2020).
[148] Simeon Spasov, Alessandro Di Stefano, Pietro Lio, and Jian Tang, "Grade: Graph dynamic embedding," arXiv preprint arXiv:2007.08060 (2020).
[149] Chuanchang Chen, Yubo Tao, and Hai Lin, "Dynamic network embeddings for network evolution analysis," arXiv preprint arXiv:1906.09860 (2019).
[150] Pengyu Cheng, Yitong Li, Xinyuan Zhang, Liqun Chen, David Carlson, and Lawrence Carin, "Dynamic embedding on textual networks via a gaussian process," in *Proceedings of the AAAI Conference on Artificial Intelligence*, Vol. 34 (2020) pp. 7562–7569.
[151] Linhong Zhu, Dong Guo, Junming Yin, Greg Ver Steeg, and Aram Galstyan, "Scalable temporal latent space inference for link prediction in dynamic social networks," IEEE Transactions on Knowledge and Data Engineering **28**, 2765–2777 (2016).

[152] John Boaz Lee, Giang Nguyen, Ryan A Rossi, Nesreen K Ahmed, Eunyee Koh, and Sungchul Kim, "Dynamic node embeddings from edge streams," IEEE Transactions on Emerging Topics in Computational Intelligence (2020), 10.1109/tetci.2020.3011432.

[153] Uriel Singer, Ido Guy, and Kira Radinsky, "Node embedding over temporal graphs," arXiv preprint arXiv:1903.08889 (2019).

[154] Srijan Kumar, Xikun Zhang, and Jure Leskovec, "Learning dynamic embeddings from temporal interactions," arXiv preprint arXiv:1812.02289 (2018).

[155] Fragkiskos Papadopoulos, Constantinos Psomas, and Dmitri Krioukov, "Network mapping by replaying hyperbolic growth," IEEE/ACM Transactions on Networking **23**, 198–211 (2014).

[156] Romualdo Pastor-Satorras, Claudio Castellano, Piet Van Mieghem, and Alessandro Vespignani, "Epidemic processes in complex networks," Reviews of modern physics **87**, 925 (2015).

[157] Sergey N Dorogovtsev and Jose FF Mendes, "Evolution of networks," Advances in physics **51**, 1079–1187 (2002).

[158] Cristopher Moore, Gourab Ghoshal, and Mark EJ Newman, "Exact solutions for models of evolving networks with addition and deletion of nodes," Physical Review E **74**, 036121 (2006).

[159] Heiko Bauke, Cristopher Moore, Jean-Baptiste Rouquier, and David Sherrington, "Topological phase transition in a network model with preferential attachment and node removal," The European Physical Journal B **83**, 519–524 (2011).

[160] Luca Becchetti, Andrea Clementi, Francesco Pasquale, Luca Trevisan, and Isabella Ziccardi, "Expansion and flooding in dynamic random networks with node churn," arXiv preprint arXiv:2007.14681 (2020).

[161] Dmitri Krioukov and Massimo Ostilli, "Duality between equilibrium and growing networks," Physical Review E **88**, 022808 (2013).

[162] Piet Van Mieghem, Huijuan Wang, Xin Ge, Siyu Tang, and Fernando A Kuipers, "Influence of assortativity and degree-preserving rewiring on the spectra of networks," The European Physical Journal B **76**, 643–652 (2010).

[163] Jean-Gabriel Young, Giovanni Petri, Francesco Vaccarino, and Alice Patania, "Construction of and efficient sampling from the simplicial configuration model," Physical Review E **96**, 032312 (2017).

[164] Tom Bannink, Remco van der Hofstad, and Clara Stegehuis, "Switch chain mixing times and triangle counts in simple random graphs with given degrees," Journal of Complex Networks **7**, 210–225 (2019).

[165] Shankar Bhamidi, Guy Bresler, and Allan Sly, "Mixing time of exponential random graphs," in *2008 49th Annual IEEE Symposium on Foundations of Computer Science* (IEEE, 2008) pp. 803–812.

[166] Ryan DeMuse, Terry Easlick, and Mei Yin, "Mixing time of vertex-weighted exponential random graphs," Journal of Computational and Applied Mathematics **362**, 443–459 (2019).

[167] Luca Avena, Hakan Güldaş, Remco van der Hofstad, Frank den Hollander, *et al.*, "Mixing times of random walks on dynamic configuration models," Annals of Applied Probability **28**, 1977–2002 (2018).

[168] Luca Avena, Hakan Güldaş, Remco van der Hofstad, and Frank den Hollander, "Random walks on dynamic configuration models: a trichotomy," Stochastic Processes and their Applications **129**, 3360–3375 (2019).

[169] Luca Avena, Hakan Güldaş, Remco van der Hofstad, Frank den Hollander, and Oliver Nagy, "Linking the mixing times of random walks on static and dynamic random graphs," arXiv preprint arXiv:2012.11012 (2020).

[170] Tamar Schlick, *Molecular modeling and simulation: an interdisciplinary guide: an interdisciplinary guide*, Vol. 21 (Springer Science & Business Media, 2010).

[171] Marco Antonio Rodríguez Flores and Fragkiskos Papadopoulos, "Similarity forces and recurrent components in human face-to-face interaction networks," Physical review letters **121**, 258301 (2018).

[172] Emmanuel Jacob and Peter Mörters, "The contact process on scale-free networks evolving by vertex updating," Royal Society open science **4**, 170081 (2017).

[173] Häggström Olle, Peres Yuval, and E Steif Jeffrey, "Dynamical percolation," in *Annales de l'Institut Henri Poincare (B) Probability and Statistics*, Vol. 33 (Elsevier, 1997) pp. 497–528.

[174] Christophe Garban, Gábor Pete, and Oded Schramm, "The scaling limits of near-critical and dynamical percolation," Journal of the European Mathematical Society **20**, 11951268 (2018).

[175] Kevin E Bassler, Erwin Frey, and RKP Zia, "Coevolution of nodes and links: Diversity-driven coexistence in cyclic competition of three species," Physical Review E **99**, 022309 (2019).

[176] Hiroki Sayama, Irene Pestov, Jeffrey Schmidt, Benjamin James Bush, Chun Wong, Junichi Yamanoi, and Thilo Gross, "Modeling complex systems with adaptive networks," Computers & Mathematics with Applications **65**, 1645–1664 (2013).

[177] Krzysztof Choromański, Michał Matuszak, and Jacek Mikisz, "Scale-free graph with preferential attachment and evolving internal vertex structure," Journal of Statistical Physics **151**, 1175–1183 (2013).

[178] Guido Caldarelli, Andrea Capocci, and Diego Garlaschelli, "A self-organized model for network evolution," The European Physical Journal B **64**, 585–591 (2008).

[179] Lia Papadopoulos, Jason Z Kim, Jürgen Kurths, and Danielle S Bassett, "Development of structural correlations and synchronization from adaptive rewiring in networks of kuramoto oscillators," Chaos: An Interdisciplinary Journal of Nonlinear Science **27**, 073115 (2017).

[180] RTAJ Leenders, "Longitudinal behavior of network structure and actor attributes: modeling interdependence of contagion and selection," Evolution of social networks **1**, 165–184 (1997).

[181] Young-Ho Eom, Stefano Boccaletti, and Guido Caldarelli, "Concurrent enhancement of percolation and synchronization in adaptive networks," Scientific reports **6**, 1–7 (2016).

[182] Marco Mancastroppa, Raffaella Burioni, Vittoria Colizza, and Alessandro Vezzani, "Active and inactive quarantine in epidemic spreading on adaptive activity-driven networks," arXiv preprint arXiv:2004.07902 (2020), 10.1103/physreve.102.020301.

[183] Genki Ichinose, Yoshiki Satotani, Hiroki Sayama, and Takashi Nagatani, "Reduced mobility of infected agents suppresses but lengthens disease in biased random walk," arXiv preprint arXiv:1807.01195 (2018).

[184] Nicholas J Gotelli, "Research frontiers in null model

analysis," Global ecology and biogeography **10**, 337–343 (2001).

[185] Georgos Siganos, Michalis Faloutsos, Petros Faloutsos, and Christos Faloutsos, "Power laws and the as-level internet topology," IEEE/ACM Transactions on networking **11**, 514–524 (2003).

[186] Luc Devroye, "Nonuniform random variate generation," Handbooks in operations research and management science **13**, 83–121 (2006).

[187] Patrick Billingsley, *Probability and measure* (John Wiley & Sons, 2008).

[188] Fragkiskos Papadopoulos, Maksim Kitsak, M Ángeles Serrano, Marián Boguná, and Dmitri Krioukov, "Popularity versus similarity in growing networks," Nature **489**, 537–540 (2012).